Nonsmooth fracture dynamics using a cohesive zone approach

Vincent Acary, Yann Monerie

INRIA

INSTITUT NATIONAL DE RECHERCHE EN INFORMATIQUE ET EN AUTOMATIQUE

Nonsmooth fracture dynamics using a cohesive zone approach

Vincent Acary — Yann Monerie

N° 6032

Octobre 2006

Thème NUM

ISSN 0249-6399 ISRN INRIA/RR--6032--FR+ENG

INRIA
RHÔNE-ALPES

Nonsmooth fracture dynamics using a cohesive zone approach

Vincent Acary *, Yann Monerie †

Thème NUM — Systèmes numériques
Projet Bipop

Rapport de recherche n° 6032 — Octobre 2006 — 56 pages

Abstract: This article is devoted to the comprehension, the prediction and the numerical simulation of dynamic fracture for a wide variety of materials and structures. The main contribution concerns the prediction of the entire fracture process from crack initiation, growth, propagation, and final rupture, to post fracture behavior such as unilateral contact and dry friction interactions between created fragments after fracture. The new Non Smooth Fracture Dynamics (NSFD) approach presented in this paper is thus based on three main features: a) a surface-volumetric multibody approach using mixed boundary conditions between each volumetric finite elements and/or rigid bodies, b) the development of a generic formulation of the cohesive zone models dedicated to a wide variety of materials and physical phenomena, and incorporating unilateral contact and Coulomb's dry friction and c) a specific nonsmooth dynamical framework based on measure differential inclusions and an associated *implicit* time–integration scheme allowing the numerical treatment of nonsmooth events such as impacts due to unilateral constraints.

Key-words: Cohesive Zone Model, Fracture Dynamics, Nonsmooth behavior, Differential inclusion, Friction, Contact Mechanics, Damage, Numerical methods

* INRIA Rhône-Alpes, Projet Bipop, `vincent.acary@inrialpes.fr`
† Institut de Radioprotection et de Sûreté Nucléaire, DPAM, BP3-13115 Saint-Paul lez Durance Cedex, France. Fax : +33 (0)4 42 19 91 66

Unité de recherche INRIA Rhône-Alpes
655, avenue de l'Europe, 38334 Montbonnot Saint Ismier (France)
Téléphone : +33 4 76 61 52 00 — Télécopie +33 4 76 61 52 52

Dynamique non régulière de la rupture par une approche de zones cohésives.

Résumé : Cet article porte sur la compréhension, la prédiction et la simulation numérique de la rupture dynamique d'une grande variété de matériaux et de structures. La contribution principale concerne la prédiction du processus de rupture complet : l'amorçage de la fissure, sa croissance, sa propagation et la rupture finale jusqu'au comportement post-rupture comme le contact unilatéral et frottement sec entre les fragments. La nouvelle approche présentée dans ce papier, dénommée "Non Smooth Fracture Dynamics" est basée sur trois points principaux: a) une approche multi-corps surfacique/volumique s'appuyant sur des conditions aux limites mixtes entre les éléments finis et les corps rigides volumiques b) le développement d'une formulation générique des modèles de zone cohésive pour une grande variété de matériaux et de phénomènes physiques et enfin c) un cadre spécifique de dynamique non régulière basé sur inclusion différentielles à mesure et un schéma d'intégration implicite permettant la résolution numérique des évolutions discontinues, telles que les impacts dus aux contraintes unilatérales.

Mots-clés : Modèle de zone cohésive, dynamique de la rupture, comportement non régulier, inclusion différentielle, frottement, Mécanique du contact, endommagement, simulation numérique

1 Introduction

This article is devoted to the comprehension, the prediction and the numerical simulation of dynamic fracture for a wide variety of materials and structures. The main contribution concerns the prediction of the entire fracture process from crack initiation, growth, propagation, and final rupture, to post fracture behavior such as unilateral contact and dry friction interactions between created fragments after fracture.

The phenomena of interest are : (i) sophisticated local behaviors in the process zone of the cracks such as elastoviscoplasticity, strong thermal coupling, reconsolidation under high pressure or high temperature, (ii) complex behaviors in the fracture plane such as contact, friction and dilatency (iii) various crack evolutions as initiation/arrest, branching, local or global mixed modes, (iv) post fracture characterizations such as overall energy balance, size of fragments, etc.

The loadings of interest are any loading leading to non negligible local inertia effects. The condition of dynamic fracture is obtained as well as for rapidly applied loading (e.g. impact) as for high speed crack propagations even under macroscopic quasi static loading [Freund, 1990].

The materials of interest are any standard deformable solids and rigid bodies, with a particular interest for pure brittle materials, elastic plastic materials and heterogeneous and graded materials. For the pure brittle materials, the difficulty is to determine the effective properties of a cracked media in which cracks propagate at a speed of the same order of magnitude than the elastic waves emitted between cracks. For the elastic plastic materials, the simulation of the competition between plastic band localization and crack initiation is the main hard challenge. Finally, for the heterogeneous and graded materials, the estimation of the equivalent effective properties together with the necessity of some local approaches yields a nontrivial problem.

Classical continuum based theories such as continuum damage models where fracture is correlated to progressive degradation of material properties (e.g. for brittle materials [Curran et al., 1987, Espinosa and Brar, 1995, Seaman et al., 1985]) or such as models based on global energy balance [Freund, 1990, Grady and Kipp, 1993] can not by definition suitably take into account discrete crack paths neither interactions between nucleations, coalescences, growths and propagations of main cracks in presence of complex microstructures. Conversely, some modern approaches are devoted to dynamic fracture in such a variety of materials. Four main classes of approaches may be distinguished : Molecular Dynamics (MD), Cohesive Zone Model (CZM) or Embedded Process Zone (EPZ), Plasticity-Free Strip (PFS) or coupled PFS-CZM and Virtual Internal Bound (VIB). Various advantages and disadvantages of each approach can be found for example in Camacho and Ortiz [1996], Zavattieri and Espinosa [2001], Thiagarajan and Misra [2004], and Wang and Nakamura [2004], and are briefly summarized in the sequel.

The Molecular Dynamics (MD) method consists in simulating the behavior of millions of atoms using some inter-atomic potentials. The capabilities and the range of applications of such a method are recalled in the recent paper of [Abraham, 2003]. For example, full *ab initio* simulations have proved that the roughness of the crack plane and the limited

crack velocity may be explained by dynamic instability arising over one third of the surface sound speed Abraham et al. [1998]. This result obtained at the lower scale confirms the observations of the pioneer work of Dally [1979] and the recent quantitative observations and interpretations of Fineberg and Mader [1999] on facies and conditions of microbranching in PMMA as an instability mechanism. In order to extend the MD approach at larger scales without drastically increasing the computational cost, Rudd and Broughton [1998] have proposed a Coarse-Grained Molecular Dynamics (CGMD) method devoted to the simulation at the micron-scale. In the same way, Abraham et al. [2000] have coupled the MD method in the crack tip zone with conventional continuum finite elements simulation in the rest of the bulk material. The MD method and its variants are not yet practical for large parametric studies due to their strong dependency on the choice of inter-atomic potentials and on the huge computational cost.

Cohesive Zone Models (CZM) (or sometimes called 'embedded process zone models') may be at the present time the most popular approaches to simulate the dynamic fracture in brittle, ductile or heterogeneous materials at any scale (grain-scale to structure). The idea of cohesive zone was first introduced by Dugdale [1960], Barenblatt [1962] and Rice [1968] concerning initially only the normal behavior (behavior during a normal separation, i.e. mode I in the rupture classification modes) at the crack tip zone. The tangential behavior (modes II and III) was first taken into account by Ida [1972] for dynamic fracture of earth's crust and by Palmer and Rice [1973] for progressive failure of an inclined layer of clay under gravity. The unilateral contact in such an approach was introduced by Frémond [1982] (no interpenetration of crack lips after fracture). Needleman [1987] has considerably extended the concept of cohesive zone by introducing new models of decohesion based on the atomistic works of Rose et al. [1981, 1983]. Those models were transformed into fracture models by Tvergaard [1990] and Needleman [1992] by the introduction of the irreversibility in the local behavior, i.e. a surface damage, and were coupled at the same time to the post fracture friction [Tvergaard, 1990] and to thermally induced residual stresses [Tvergaard, 1991]. It was then possible to simulate crack initiation without any ad hoc criterion, propagation (crack path emerges naturally from the external loading without any convenient assumption on the crack plane) and final rupture by incorporating CZM at interfaces between each element of a finite elements discretization [Costanzo and Walton, 1997, Needleman and Rosakis, 1999, Xu and Needleman, 1994]. This multibody cohesive framework has shown its ability to predict complete fracture process of elastic-plastic materials under quasi static loading [Needleman, 1990, Tvergaard and Hutchinson, 1992] or submitted to crack tip instabilities [Xu and Needleman, 1994], of brittle materials under impact [Camacho and Ortiz, 1996, Zavattieri and Espinosa, 2001], of elastic viscoplastic materials [Siegmund and Needleman, 1997], of composite materials [Needleman and Rosakis, 1999, Siegmund et al., 1997, Xu et al., 1997] and of graded materials [Wang and Nakamura, 2004, Zhang and Paulino, 2005]. Most of the results obtained in this framework were given in two dimensions; in three dimensions, the feasibility of using such a multibody cohesive framework to simulate dynamic fracture from initiation to rupture was established by Monerie [2000] and Pandolfi et al. [2000]. From the point of view of cohesive zone modeling, one distinguishes the so-called intrinsic models

(CZM with initial compliance) and extrinsic models (CZM without any initial compliance). Recent comparisons between intrinsic and extrinsic models for dynamic crack branching and for dynamic crack instability can be found respectively in Falk et al. [2001] and in Kubair and Geubelle [2003]. From the point of view of numerical implementations, two main choices are possible. CZM could be implemented as mixed boundary conditions (MBC) between volumetric finite elements or as cohesive elements (i.e. surface finite elements). This last class of implementation is referred to cohesive-volumetric finite element (CVFE) and tends to be widely developed [Geubelle and Baylor, 1998]. For the CVFE scheme, the relative position of cohesive elements between volumetric elements seems to have a strong influence in the case of finite slips. The MBC scheme does not meet this difficulty. Since we are interested in this paper by a modeling and a numerical implementation of dynamic fracture problems in the most general case, we retain in what follows the MBC scheme. However, the 'cohesive-volumetric finite element' name being well-known and clear, it is employed in this paper, but having the meaning of a surface-volumetric multibody approach using mixed boundary conditions between each volumetric finite elements.

Two main limitations of the CZM models are their possible instability due to their softening character [Chaboche et al., 2001, Monerie and Acary, 2001] and their inability to predict crack opening in the case of elastic-perfectly plastic materials when the ratio between the peak traction stress of the CZM and the yield stress of the bulk material is lower than about 3.0 [Tvergaard and Hutchinson, 1996]. The first apparent limitation is deeply further studied in this article. The second one has conducted to the development of Plasticity-Free Strip (PFS) model by Suo et al. [1993]. In this model, a thin elastic strip is incorporated between the crack and the surrounding plastic zone and the crack propagation is governed by a local criterion on the energy release rate. Due to the sensitivity of this model to the thickness of the PFS and this limitation when the crack separation stress is small, Wei and Hutchinson [1999] have developed an EPZ-PFS unified model which progressively evolves from one model to the other depending on material parameters. This model is powerful for a wide range of elastic plastic parameters but has the disadvantage to incorporate both parameters of an EPZ model and of a PFS model. Finally, the PFS model or the EPZ-PFS unified model requires a prior definition of the crack path.

The Virtual Internal Bound (VIB) model, developed by Gao and Klein [1998] and Klein and Gao [1998], consists in incorporating the fracture law directly into the constitutive model of standard finite elements schemes. In each continuum finite element, randomly distributed material particles are connected by a random spatial network of the phenomenological cohesive internal bonds. The macroscopic behavior of this kind of representative volume element from the point of view of atomistic fracture is obtained by equating the strain energy function on the continuum level to the potential energy stored in the cohesive internal bonds. The corresponding fracture law depends on the local deformation around the crack tip. Althoughthe VIB model has been successfully used (see for instance by Thiagarajan and Misra [2004]), to simulate fracture of anisotropic media, it seems to be unstable in the case of heterogeneous materials and requires a large computational cost.

The aim of this article is to simulate the fracture dynamics (from initiation to post-fracture) of a wide variety of materials ranging from rigid, brittle or ductile homogeneous bodies to heterogeneous materials without a prior knowledge of crack paths and including complex phenomena such as friction or wear on the crack lips possibly with finite slips. Regarding advantages and disadvantages of various methods, the cohesive zone approaches are ideal candidates to achieve this goal without supercomputer facilities. An additional motivation for the choice of CZM is the clear mechanical sense of the two main parameters of CZM: the peak traction stress drives the initiation of fracture and the cohesive energy (or equivalently the critical energy release rate or critical stress intensity factor) drives the crack propagation independently of the specific form of the traction-separation curve [Monerie et al., 1998, Zavattieri and Espinosa, 2001]. The new Non Smooth Fracture Dynamics (NSFD) approach presented in this paper is thus based on three main features:

1. a surface-volumetric multibody approach using mixed boundary conditions between each volumetric finite elements and/or rigid bodies (Figure 1), sometimes wrongly called (when no confusion is possible) cohesive-volumetric finite element method;
2. the development of a generic formulation of the cohesive zone models dedicated to a wide variety of materials and physical phenomena, and incorporating unilateral contact and Coulomb's dry friction; such a formulation is referred in this paper to 'Enhanced Cohesive Zone Models' (ECZM) ans is associated with numerical techniques arising from the mathematical programming community;
3. a specific non smooth dynamical framework based on measure differential inclusions and an associated *implicit* time–integration scheme allowing the numerical treatment of non smooth events such as impacts due to unilateral constraints; this scheme is referred as 'Non Smooth Contact Dynamics' (NSCD).

As we will show, these two last features considerably improve the classical CVFE scheme in the context of the dynamic fracture. As an example of this improvement, one can consider the importance of the unilateral contact in the cohesive zone models, which ensure the non penetrability of the volumetric finite elements when the stress waves lead to compression, and the difficulty to numerically integrate such unilateral constraints within a dynamic framework when nonsmooth events are expected.

Outline Section 2 is dedicated to the presentation of the enhanced cohesive zone concept. A generic formulation is presented and the link with other well-know cohesive zone models is made. Finally, the particular interest for this model is described. Section 3 is devoted to some practical aspects of using cohesive model. The question of the uniqueness of the solution, the equivalence and the stability of extrinsic and intrinsic models is tackled. To complete this section, the prominent role of the dynamics as a relaxation ingredient is evoked. In Section 4, the nonsmooth dynamical framework is settled in terms of differential measure formulation. Some comments and explanations are given to justify this approach. The numerical time-integration and the resolution of the one-step discretized problem is presented in Section 5. Section 6 concludes the paper.

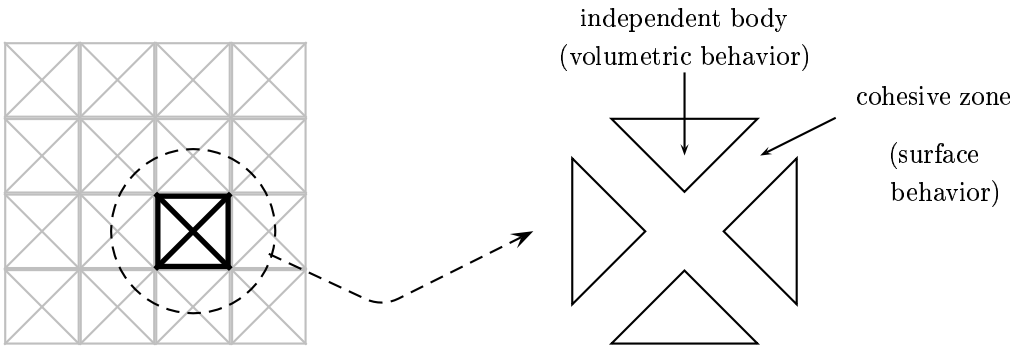

Figure 1: The surface-volumetric multibody approach: each mesh is considered as an independent body connected to each other using cohesive zone model as mixed boundary conditions.

2 Enhanced Cohesive Zone Models: from crack initiation to post fracture

2.1 Notation

In this section, the main notation is introduced. The attention is focused on the normal/tangent decomposition of the variables across the interface between two bodies.

For $i = 1, 2$, let $\Omega^i \subset \mathbb{R}^d$ $(d = 2, 3)$ being two bodies with sufficiently smooth boundary $\partial\Omega^i$ and subjected to body forces $\rho^i b^i$ and external forces T^i, where rho^i is the mass density. The boundary $\partial\Omega^i$ is composed of three distinct parts: the potential contact zone Γ_c^i between Ω^i and the outer, the zone $\partial\Omega_U^i$ where displacements are prescribed, and the zone $\partial\Omega_F^i$ where forces are prescribed, with $\partial\Omega^i = \overline{\Gamma_c^i} \cup \overline{\partial\Omega_U^i} \cup \overline{\partial\Omega_F^i}$. Under the small displacements assumption, the potential contact zone between the two bodies and its unit outer vector can be respectively defined as $\Gamma_c = \Gamma_c^1 = \Gamma_c^2$, and $n(x) = n^1(x) = -n^2(x)$ ($n^i(x)$ being the unit outer vector of Ω^i). We denote by $u = \{u^1, u^2\}$ the displacement field in $\Omega^1 \cup \Omega^2$, and by $[u] = u^2 - u^1$ the displacement jump across the boundary Γ_c. The internal forces associated to these variables are the stress field $\sigma = \{\sigma^1, \sigma^2\}$ in $\Omega^1 \cup \Omega^2$ and the contact force R on Γ_c (Figure 2). In what follows, the subscripts N and T denote respectively normal and tangential components of the total force ($\mathsf{R} = \mathsf{R}_N n + \mathsf{R}_T$), of the cohesive force ($\mathsf{R}^{coh} = \mathsf{R}_N^{coh} n + \mathsf{R}_T^{coh}$) and of the displacement jump ($[u] = u_N n + u_T$).

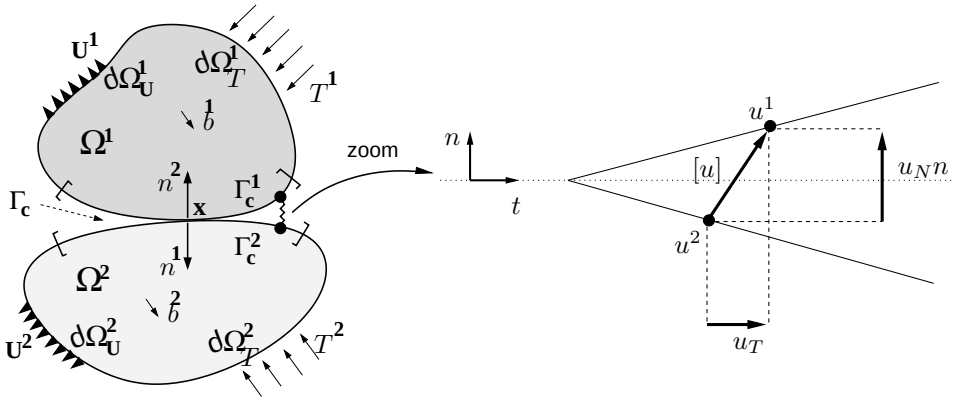

Figure 2: Sketch of cohesive zone model and notations: two bodies in interaction (left), and details across the interface including the normal/tangent decomposition of the displacement jump (right).

2.2 Generic formulation

The two main cohesive failure models used in the literature are the potential-based law of Tvergaard [1990] and Xu and Needleman [1994] and the linear law of Camacho and Ortiz [1996] and Ortiz and Pandolfi [1999]. During the four past decade, many other models were also developed; to cite a few of them, Dugdale [1960], Barenblatt [1962], Palmer and Rice [1973], Needleman [1987], Rice and Wang [1989], Needleman [1990], Tvergaard and Hutchinson [1992], Michel et al. [1992], Michel and Suquet [1994], Allix et al. [1995], Chaboche et al. [1997], Geubelle and Baylor [1998], Raous et al. [1999], Varias and Massih [2002], Jin et al. [2002], Espinosa and Zavattieri [2003], and Li et al. [2006]. These models attempt to conveniently describe the evolution of the cohesive force R^{coh} together with the displacement jump $[u]$ according to the type of material considered by their authors: brittle or ductile homogeneous materials, heterogeneous materials, functionally graded materials, particle-matrix interfaces, adhesive joints, concrete, clay, etc. For an extensive review on the models see Monerie [2000], Chandra et al. [2002], and Perales [2005]. These models have various *shape*, various mechanical parameters; they are based on various formulations (a simple law, a potential-based model, a thermodynamics-based model); they are sometimes dedicated only to the normal behavior of the cohesive zone, sometimes only to its tangential behavior, or sometimes both. Sometimes, the effects of the unilateral or regularized contact, the effect of Coulomb's friction before, during, or after decohesion are included in the model although most of the model neglect them.

In this paper, we claim firstly, that *all* of these models can be written in a unique formulation. Secondly, that they can be coupled with a non regularized unilateral contact and Coulomb's friction model, including a progressive transition from a perfect cohesive zone to

a pure frictional contact zone. This type of formulation is called 'enhanced cohesive zone model' (ECZM).

This formulation, based on the works of Raous et al. [1999] and Raous and Monerie [2001] on the soft coupling between adhesion and frictional contact, is given by equations (1)-(4) for the case of *intrinsic* models.

$$-\left(\mathsf{R}_N + \mathsf{R}_N^{coh}\right) \in \partial I_{\mathbb{R}^+}(u_N) \tag{1}$$

$$\left(\mathsf{R}_T + \mathsf{R}_T^{coh}\right) \in \partial\left(\mu\,\kappa(\beta)|\mathsf{R}_N + \mathsf{R}_N^{coh}|\parallel \dot{u}_T \parallel\right) \tag{2}$$

$$\mathsf{R}^{coh} = K(\beta)\cdot[u] \qquad \text{and} \qquad g\left(\dot{\beta},\,\beta,\,u_N,\,u_T\right) = 0 \tag{3}$$

where I_X is the indicator function of the set X, μ is the Coulomb's friction coefficient, β is a variable of surface damage, $\kappa(\beta)$ and g are given functions, and $K(\beta)$ is a second-order tensor giving the progressive softening of the surface behavior during the decohesive process:

$$K(\beta) = \beta\left(C_N n\otimes n + C_T\frac{u_T\otimes u_T}{\|u_T\|^2}\right), \tag{4}$$

the quantities C_N and C_T being respectively the initial normal and tangential 'stiffnesses' (or the so-called 'initial slope') of the cohesive zone. The surface damage parameter β, initially introduced by Frémond [1987, 1988], and the function $\kappa(\beta)$ allow a soft transition from the decohesion law described by (3) to the contact-friction law given by (1) and (2): $\beta = 1$ when the cohesive zone is undamaged, $0 < \beta < 1$ when the cohesive zone is partially damaged, and $\beta = 0$ when the cohesive zone is fully damaged. Usually, in order to avoid any friction before the beginning of the decohesive process, the function $\kappa(\beta)$ has to be equal to zero when β is still equal to 1; and, in order to be in a pure frictional contact state after complete decohesion, the function $\kappa(\beta)$ has to be equal to 1 when β vanishes. The function g is often describing a softening behavior or a pure brittle one, and leads to a decrease of β from a initial value lying between 1 and 0 to zero.

In the case of *extrinsic* models, the couple of equations in (3) has to be slightly modified in order to give a direct description of R^{coh} without involving a linear function of u_N through the 'stiffness' tensor $K(\beta)$. The most simple choice is to postulate that the cohesive force does not depend explicitly on the displacement jump $[u]$ but only on β. For instance, the following form can be chosen

$$\mathsf{R}^{coh} = \beta\,\mathsf{R}_{\max}^{coh} \qquad \text{and} \qquad \tilde{g}\left(\dot{\beta},\,\beta,\,u_N,\,u_T\right) = 0 \tag{5}$$

where $\mathsf{R}_{\max}^{coh}$ is the maximum adhesive force. In a more general setting, *extrinsic* models can be written as function of β such as

$$\mathsf{R}^{coh} = \Upsilon\left(\beta\right) \qquad \text{and} \qquad \tilde{g}\left(\dot{\beta},\,\beta,\,u_N,\,u_T\right) = 0 \tag{6}$$

where Υ is a given function associated with the shape of the cohesive force. An explicit dependence on $[u]$ would involve an equivalent tangent stiffness which contradicts the assumption of the extrinsic models. Nevertheless, an implicit dependence on $[u]$ is given throughout the function $\tilde{g}$.

More generally, the cohesive zone model for the normal part can be expressed by the following inclusion

$$\mathsf{R}_N \in \partial_{u_N} \Psi(u_N, \beta), \tag{7}$$

where $\Psi(u_N, \beta)$ is the free energy of the interface which can be chosen of the form:

$$\Psi(u_N, \beta) = \psi(\beta, u_N) + I_{\mathbb{R}^+}(u_N) + I_{[0,1]}(\beta). \tag{8}$$

Comparing to the equation (1), the equations (7) and (8) yield to the following form for the cohesive force,

$$\mathsf{R}_N^{coh} = \partial_{u_N} \psi(\beta, u_N). \tag{9}$$

If the function ψ is sufficiently regular, any choice of ψ such that $\dfrac{\partial^2 \psi(\beta, u_N)}{\partial^2 u_N} = 0$ would lead to an extrinsic model. Concerning the evolution of β with $[u]$, the second law in (3) can also be expressed in a slight different way by considering a law of the form:

$$\dot{\beta} = \partial_\chi \Lambda(\chi), \tag{10}$$

where χ is the thermodynamical force associated to the damage variable by

$$\chi = \partial_\beta \Psi(u_N, \beta). \tag{11}$$

Such a model proposed in the pioneering work of Frémond [1987, 1988] has been studied from a mathematical point of view by Point [1988], and Point and Sacco [1998]. The function Λ, which can be understood as a pseudo-potential of dissipation, may be chosen as the indicatrix function of a set C. In this case, we obtain a brittle behavior for the interface.

Most of intrinsic cohesive zone model of the literature are defined by the couple of equations (3) and (4), and in what follows, for a given CZM defined by these relations, the formulation (1)-(4) is then called the ECZM formulation of the initial CZM (3)-(4).

2.3 Some particular examples

In this section, the ECZM formulation (1)-(4) is detailed for two particular cases of intrinsic models. The first model is the ECZM formulation of the law proposed by Tvergaard [1990], which is one of the most wisespread cohesive zone model in the literature. The second model is a new model proposed by Perales et al. [2005], which will be used later in the remaining part of this paper.

2.3.a The standard cohesive zone model of Tvergaard [1990]

The standard Tvergaard's cohesive law consists in introducing the irreversibility of the interfacial behavior in the law of Needleman [1987]. In two dimensions, this model is based on a non-dimensional parameter related to the displacement jump $[u]$:

$$\lambda = \sqrt{\left(\frac{u_N}{\delta_N}\right)^2 + \left(\frac{u_T}{\delta_T}\right)^2}, \tag{12}$$

and on a normalized piecewise quadratic function:

$$F(\lambda) = \frac{27}{4}\mathsf{R}^{coh}_{\max}(1-\lambda)^2 \text{ for } 0 \leqslant \lambda \leqslant 1, \quad F(\lambda) = 0 \text{ otherwise}, \tag{13}$$

where δ_N and δ_T are critical values at which the interface is broken, and $\mathsf{R}^{coh}_{\max}$ is the maximum normal traction reached before the onset of the decohesion (the peak stress). The normal traction R^{coh}_N and the tangential traction R^{coh}_T are given by:

$$\mathsf{R}^{coh}_N = \frac{u_N}{\delta_N}F\left(\widetilde{\lambda}\right) \qquad \text{and} \qquad \mathsf{R}^{coh}_T = i\frac{u_T}{\delta_T}F\left(\widetilde{\lambda}\right), \tag{14}$$

where i is a parameter coupling normal and shear tractions and $\widetilde{\lambda}$ describes the irreversibility of this cohesive zone model. Denoting by $\lambda_{\max}$ the maximum value ever reached by $\widetilde{\lambda}$, we have:

$$\widetilde{\lambda} = \max\{\lambda,\, \lambda_{\max}\}. \tag{15}$$

From the point of view of the ECZM formulation, this well-known model can be reformulated and closely coupled with unilateral contact and Coulomb's friction using formulation (1)-(4), with:

$$C_N = \frac{27}{4}\frac{\mathsf{R}^{coh}_{\max}}{\delta_N} \qquad \text{and} \qquad C_T = i\frac{27}{4}\frac{\mathsf{R}^{coh}_{\max}}{\delta_T} \tag{16}$$

$$g\left(\dot{\beta},\, \beta,\, u_N,\, u_T\right) = \beta - \min\left\{(1-\lambda)^2,\, \beta_{\min}\right\}, \tag{17}$$

where $\beta_{\min}$ the minimum value reached by β.

In this compact formulation, the quantity β has the meaning of a damaged 'stiffness' over an initial 'stiffness' (β decreases from 1 to 0 with $\|[u]\|$), and the standard Tvergaard's law is thus extended to frictional contact. This extension can be completed by incorporating a progressive transition from cohesion to friction giving a particular form to the function $\kappa(\beta)$, as:

$$\kappa(\beta) = (1-\beta)^s \quad \text{with } s = 1,\, 2 \text{ or } 3, \text{ for example.} \tag{18}$$

The resulting ECZM is plotted in Figure 3, and it should be noticed that the cohesion-friction progressive transition incorporates in the decohesion process an energy dissipated by friction, which stays very small until the failure is not completely reached.

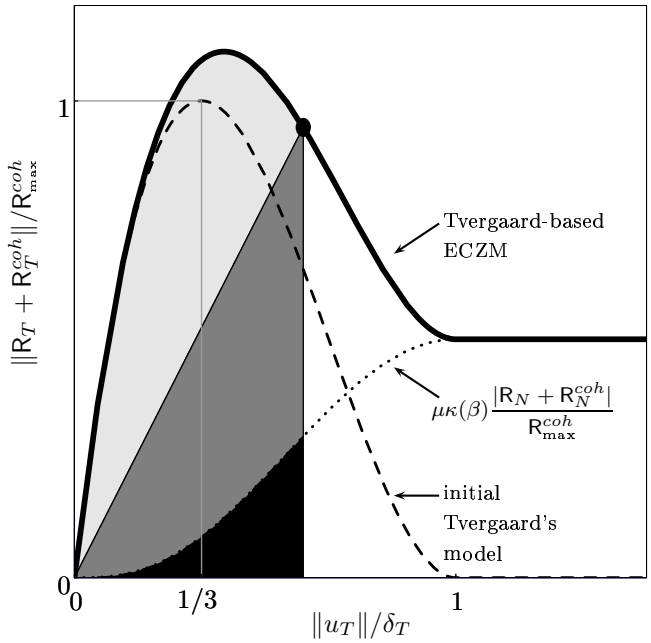

Figure 3: Enhanced version of the standard Tvergaard's cohesive law introducing a soft coupling with unilateral contact and Coulomb's friction (formulation (1)-(4)). Normalized tangential traction $\|\mathsf{R}_T + \mathsf{R}_T^{coh}\|/\mathsf{R}_{\max}^{coh}$ versus normalized tangential displacement jump $\|u_T\|/\delta_T$ for $i = 1$ in the case of unilateral contact ($u_N = 0$ and $(\mathsf{R}_N + \mathsf{R}_N^{coh}) \geqslant 0$ constant, quantity $\mu\kappa(\beta)$ defined by (18) with $s = 3$), and various energies at a given decohesion state: energy dissipated during the decohesive process (light gray area), elastic stored energy (dark gray area), energy dissipated by friction (black area).

2.3.b A new 'enhanced cohesive zone model'

In order to underline the relevance of the ECZM formulation (1)-(4), a second intrinsic model is here detailed. This model, previously proposed by Perales et al. [2005], derives from a surface damage law initially proposed by Michel and Suquet [1994] as:

$$g\left(\dot{\beta},\, \beta,\, u_N,\, u_T\right) = \beta - \min\left\{\beta_0\left(D_{[0,\delta_c[}\left(\|[u]\|\right) + D_{[\delta_c,3\delta_c[}\left(\|[u]\|\right)\frac{3\delta_c - \|[u]\|}{\delta_c + \|[u]\|}\right),\, \beta_{\min}\right\}, \tag{19}$$

where $D_{[a,b[}(x)$ is the door function equal to 1 if $x \in [a, b[$ and equal to 0 otherwise, δ_c is a critical displacement jump and β_0 is an initial value of the surface damage parameter β.

Anticipating on Section 3.1, it should be already mentioned that the main feature of this ECZM, from the point of view of the cohesive part of the law, is to have its maximum negative slope (maximum slope in the softening part) just at the end of the decohesion, i.e. at the critical displacement where the failure occurs. As we will latter underline, the

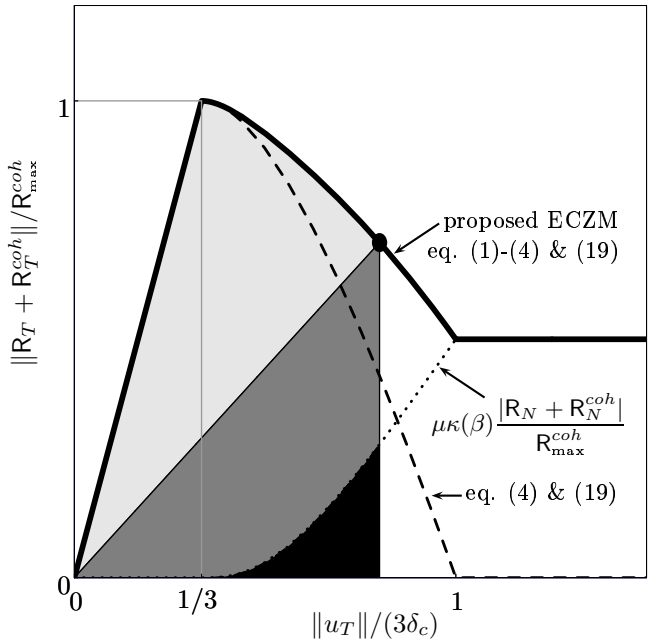

Figure 4: The Enhanced Cohesive Zone Model used in this paper (formulation (1)-(4) and equation (19)). Normalized tangential traction $\|\mathsf{R}_T + \mathsf{R}_T^{coh}\|/\mathsf{R}_{\max}^{coh}$ versus normalized tangential displacement jump $\|u_T\|/(3\delta_c)$ in the case of unilateral contact ($u_N = 0$ and $(\mathsf{R}_N + \mathsf{R}_N^{coh}) \geqslant 0$, quantity $\mu\kappa(\beta)$ defined by (18) with $s = 3$), and various energies at a given decohesion state: energy dissipated during the decohesive process (light gray area), elastic stored energy (dark gray area), energy dissipated by friction (black area).

instabilities related to the softening behavior of the cohesive laws are correlated to this maximum negative slope: if instabilities are suspected, the smaller the cohesive force at the maximum negative slope, the better the energy balance. From this point of view, the cohesive law incorporated in this ECZM belongs to the 'most stable cohesive zone models'. This appellation is here enforced by the fact that the proposed cohesive law has a non negative slope at the peak stress: the suspected instabilities can never occur at the onset of decohesion. The other main feature of this ECZM is that any energy is dissipated by friction before the onset of decohesion. This situation is illustrated in Figure 4.

The effects of the strict unilateral contact and of the progressive transition from decohesion to friction incorporated in the ECZM-formulation (1)-(4) are underlined in Figure 5.

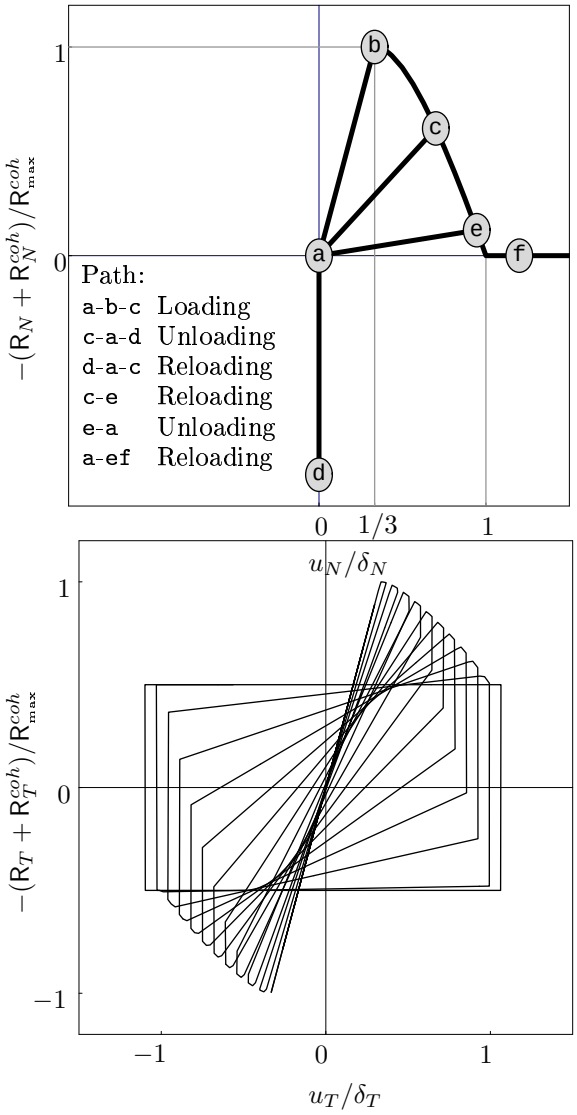

Figure 5: The Enhanced Cohesive Zone Model used in this paper (formulation (1)-(4) and equation (19)). Left: normalized normal traction $(\mathsf{R}_N+\mathsf{R}_N^{coh})/\mathsf{R}_{\max}^{coh}$ versus normalized normal displacement jump u_N/δ_T during a traction-compression loading path ($u_T = 0$ and $(\mathsf{R}_T + \mathsf{R}_T^{coh}) = 0$). Right: normalized tangential traction $(\mathsf{R}_T + \mathsf{R}_T^{coh})/\mathsf{R}_{\max}^{coh}$ versus normalized tangential displacement jump u_T/δ_T during cyclic loading with unilateral contact ($u_N = 0$ and $(\mathsf{R}_N + \mathsf{R}_N^{coh}) \geqslant 0$, quantity $\mu\kappa(\beta)$ defined by (18) with $s = 3$).

2.4 Interests and comments

As shown in the two examples above, the ECZM formulation has many advantages. It is a very compact formulation of any cohesive closely coupled with unilateral contact and Coulomb's friction law and with a soft transition from the cohesive behavior. It should be underlined that in absence of cohesive force (i.e. $\mathsf{R}_N^{coh} = \mathsf{R}_T^{coh} = 0$ in equations (1) and (2)) the standard Signorini-Coulomb relationships are obtained:

$$\mathsf{R}_N \geqslant 0, \qquad u_N \geqslant 0, \qquad \mathsf{R}_N u_N = 0, \tag{20}$$

$$\|\mathsf{R}_T\| \leqslant \mu|\mathsf{R}_N|, \quad \begin{cases} \|\mathsf{R}_T\| < \mu|\mathsf{R}_N| \Rightarrow \dot{u}_T = 0, \\ \|\mathsf{R}_T\| = \mu|\mathsf{R}_N| \Rightarrow \exists \lambda \geqslant 0,\ \dot{u}_T = -\lambda \mathsf{R}_T. \end{cases} \tag{21}$$

In these Signorini-Coulomb relationships, the quantity $\kappa(\beta)$ do not appear due to the fact that the condition $\mathsf{R}_N^{coh} = \mathsf{R}_T^{coh} = 0$ impose $\beta = 0$, and $\kappa(\beta = 0) = 1$ as mentioned in section 2.2.

This coupling between a cohesive law, unilateral contact and Coulomb's friction law is of great interest in dynamics fracture. On one hand, the friction plays a determinant role in the fracture of heterogeneous materials: the mismatch between the Poisson coefficient of each phase leads to a mixed mode fracture at the interface between the constituents, and the resulting friction at the interface takes an important place in the overall toughness of the composite, during the fracture process and after the complete decohesion of the interface (e.g., fiber pull-out in fibrous composites). The role of this friction is increased for dynamical loadings, for which intersonic crack growth along the interface can occur [Needleman and Rosakis, 1999, Xu et al., 2003]. On the other hand, the unilateral contact plays a determinant role in the fracture of heterogeneous materials as well as homogeneous materials. For heterogeneous materials, the unilateral contact allows one to conveniently estimate the normal contact force R_N, which determines the conditions of sticking or frictional sliding in the Coulomb's law (21). For homogeneous materials in the context of fracture dynamics treated by CZM embedded in a continuum simulation, incorporating unilateral conditions in the CZMs is quite useful: compressive waves can induce interpenetration of volumetric finite elements. Convenient simulations of fracture dynamics using cohesive zone models have to take into account unilateral contact conditions and friction. This is the main characteristic of the proposed ECZM formulation.

Another feature of the (1)-(4) ECZM formulation is that the crack initiation and propagation are outcomes of the simulation and are not obtained using any *ad hoc* criteria. This particularity comes both from the CZM incorporated in the ECZM formulation and from the CVFE scheme.

As far as the interest of the ECZM formulation (1)-(4) is concerned, we finally underline that this formulation is open enough to be completed with various surface mechanisms as dilatency, wear or 'undrained cracks'. This last point allows one to simulate the presence of

a pressurized gas of fluid at pressure p inside the growing cracks. In the ECZM formulation, a normal pressure can be taken into account on the lips of a created crack, i.e. only when the cohesive zone is broken ($\beta = 0$), by substituting the quantity,

$$\mathsf{R}^{coh} + pnD_{[0,0]}(\beta) \tag{22}$$

to R^{coh} in equation (3).

3 Practical use of Enhanced Cohesive Zone Models and Cohesive-Volumetric Finite Element method

This section is devoted to the analysis of the main bias of the cohesive zone models that can affect the global response of a structure. The two main features of a cohesive zone model that can induce a non desirable effect in the numerical simulations are:

- the softening behavior which leads to the ill-posedness of the rate boundary value problem,
- the internal length that has to be tailored according to the work of separation or fracture energy, the maximal stress reached at the cohesive zone, the bulk material properties and the spatial discretization.

In the sequel, the first point is detailed with the help of a mathematical result of Monerie and Acary [2001] and its physical meaning previously proposed by Chaboche et al. [2001]. The second point is extensively debated in the literature where numerous results can be found. At the end of this section, a new result giving a lower bound for the initial slope of the intrinsic cohesive zone models is provided.

3.1 The dynamical relaxation of weakening behavior

3.1.a A condition of uniqueness

The softening behavior of the cohesive zone model rises to an ill-posed rate boundary value problem. A discontinuity in the response can be observed during quasi-static numerical simulations. In order to give a convenient mathematical framework to the comprehension of these "solution jumps", we propose in this section a condition of existence and uniqueness to the quasi-static separation problem of two elastic bodies Ω^1 et Ω^2 (see Figure 2) bonded by a rate-insensitive cohesive zone model without friction. This result was first obtained by Monerie [2000] and Monerie and Acary [2001].

Let us recall the standard notation of classical spaces of vector-valued functions. The spaces $L^p(\Omega), 1 < p < +\infty$ are defined by the spaces of Lebesgue-measurable functions such that $\|f\|_{L^p(\Omega)} = (\int_\omega |f|^p \, dx)^{1/p} < +\infty$ and L^∞ is the space of Lebesgue-measurable functions such that $\operatorname{ess\,sup} |f| < +\infty$. The Sobolev's spaces of order m are denoted by

$W^{m,p}(\Omega) = \{v \in L^p(\Omega) | D^\alpha v \in L^p(\Omega), \forall |\alpha| \leqslant m\}$ and are associated to the following norm $\|v\|_{W^{m,p}(\Omega)} = (\sum_{|\alpha| \leqslant m} \|D^\alpha v\|^p_{L^p(\Omega)})^{1/p}$. Finally, the standard notation $H^m = W^{m,2}$ is also used.

Without any loss of generality, vanishing prescribed displacements are considered on the boundaries of Ω^1 et Ω^2. The following sets are introduced in three dimensions, that is for $\Omega^i \subset \mathbb{R}^3$:

$$V^i = \left\{ v^i \in \left[H^1(\Omega^i)\right]^3 ;\ v^i = 0 \text{ a.e. on } \partial\Omega^i_U \right\} \qquad (i = 1, 2), \tag{23}$$

$$\mathcal{K} = \left\{ v = (v^1, v^2) \in V ;\ v_N \geqslant 0 \text{ a.e. on } \Gamma_c \right\} \tag{24}$$

$$V = V^1 \times V^2, \qquad \text{and} \qquad H = L^\infty(\Gamma_c). \tag{25}$$

The body forces and the surface forces are assumed to have a sufficient regularity:

$$\rho b = \left(\rho^1 b^1, \rho^2 b^2\right) \in W^{1,2}(0, T; [L^2(\Omega^1)]^3 \times [L^2(\Omega^2)]^3) \tag{26}$$

$$T = \left(T^1, T^2\right) \in W^{1,2}(0, T; [L^2(\partial\Omega^1_F)]^3 \times [L^2(\partial\Omega^2_F)]^3). \tag{27}$$

The function ϕ is defined by (Einstein's convention):

$$(\phi, v) = \int_{\Omega^i} \rho^i b^i \cdot v^i dx + \int_{\partial\Omega^i{}_F} T^i \cdot v^i ds, \quad \forall v \in V. \tag{28}$$

The assumptions (26) and (27) ensure that $\phi \in W^{1,2}(0, T; V)$. Finally, we denote by $\gamma^i u = \gamma|_{\Gamma_c} u^i$ the trace of u^i on Γ_c (for $i = 1, 2$).

Assuming a rate-independent intrinsic cohesive zone model, the left equation of (3) can be rewritten as

$$\beta = g^\star([u]), \tag{29}$$

where $g^\star \in H$, and the cohesive force R^{coh} can be described as a function ξ of $[u]$:

$$\xi([u]) = \mathsf{R}^{coh}([u]) = K \circ g^\star([u]) \cdot [u], \tag{30}$$

with $\xi : [L^2(\Gamma_c)]^3 \to [L^2(\Gamma_c)]^3$.

Without any friction, and with initial conditions $u_0 \in \mathcal{K}$ and $\beta_0 \in H \cap [0, 1]$, the quasi-static frictional contact problem of Cocu et al. [1996] can be extended to the cohesive case yielding the following variational problem:

$$a(u, v - u) + \int_{\Gamma_c} \xi([u]) \cdot ([v] - [u])\, ds - (\phi, v - u) \geqslant 0, \forall v \in \mathcal{K}, \tag{31}$$

where

$$a(u, v) = \int_{\Omega^i} \varepsilon(u^i) : A^i : \varepsilon(u^i) dx. \tag{32}$$

The following theorem of existence and uniqueness of a solution to the problem (31) can be given:

Theorem 1 *The application* $\tilde{s} : k \to \xi([u(k)])$ *where* $u(k) \in \mathcal{K}$ *is the solution of:*

$$a(u, v-u) - (\phi, v-u) + \int_{\Gamma_c} k \cdot ([v]-[u])ds \geqslant 0 \quad \forall v \in \mathcal{K}, \tag{33}$$

admits a unique fixed point $\bar{k}$ *if* $\lambda^2 c_1/m < 1$. *The displacement* $u(\bar{k})$ *is thus the solution of the problem (31).*

1 **proof**
Let $u(k_1)$ be the solution of (33) for $k = k_1$, and $u(k_2)$ be the solution of (33) for $k = k_2$. For a given k, the existence and the uniqueness of a solution to the problem (33) is a classical result in variational inequalities [Kikuchi and Oden, 1988]. By substituting $v = u(k_2)$ in (33) for $k = k_1$, and $v = u(k_1)$ for $k = k_2$, one obtains after summation:

$$a(u(k_1) - u(k_2), u(k_1) - u(k_2)) \leqslant \int_{\Gamma_c} (k_2 - k_1) \cdot ([u(k_1)] - [u(k_2)])ds.$$

The coercivity of a (constant m, Korn's inequality and positive measure of the part of the boundary where displacements are prescribed), and the Schwarz's inequality for the scalar product on $[L^2(\Gamma_c)]^3$, lead to:

$$m\|u(k_1) - u(k_2)\|^2_{H^1(\Omega)} \leqslant \|k_2 - k_1\|_{L^2(\Gamma_c)} \|[u(k_1)] - [u(k_2)]\|_{L^2(\Gamma_c)}. \tag{34}$$

By the definition of the displacement jump, the first triangular inequality gives:

$$\|[u(k_1)] - [u(k_2)]\|_{L^2(\Gamma_c)} \leqslant \|\gamma^2 u(k_1) - \gamma^2 u(k_2)\|_{L^2(\Gamma_c)} + \|\gamma^1 u(k_1) - \gamma^1 u(k_2)\|_{L^2(\Gamma_c)}. \tag{35}$$

The continuity of the injection from $[H^{1/2}(\partial\Omega^i)]^3$ to $[L^2(\Gamma_c)]^3$ and of the trace application from $[H^1(\Omega)]^3$ on $[H^{1/2}(\partial\Omega^i)]^3$ ensures that there exist two positive constants λ^i $(i = 1, 2)$ such that:

$$\|\gamma^i u(k_1) - \gamma^i u(k_2)\|_{L^2(\Gamma_c)} \leqslant \lambda^i \|u(k_1) - u(k_2)\|_{H^1(\Omega)}, \quad \text{for } i = 1, 2. \tag{36}$$

Introducing $\lambda = \lambda^1 + \lambda^2 > 0$, and combining inequalities (35) and (36), one obtains:

$$m\|u(k_1) - u(k_2)\|^2_{H^1(\Omega)} \leqslant \lambda \|k_2 - k_1\|_{L^2(\Gamma_c)} \|[u(k_1)] - [u(k_2)]\|_{H^1(\Omega)}. \tag{37}$$

Moreover, assuming that ξ is Lipschitz continuous (constant c_1), we obtain:

$$\begin{aligned} \|\tilde{s}(k_1) - \tilde{s}(k_2)\|_{L^2(\Gamma_c)} &\leqslant c_1 \|[u(k_1)] - [u(k_2)]\|_{L^2(\Gamma_c)}, \\ &\leqslant \lambda c_1 \|u(k_1) - u(k_2)\|_{H^1(\Omega)}. \end{aligned}$$

Finally, the equation (34) gives:

$$\|\tilde{s}(k_1) - \tilde{s}(k_2)\|_{L^2(\Gamma_c)} \leqslant \frac{\lambda^2 c_1}{m} \|k_2 - k_1\|_{L^2(\Gamma_c)}.$$

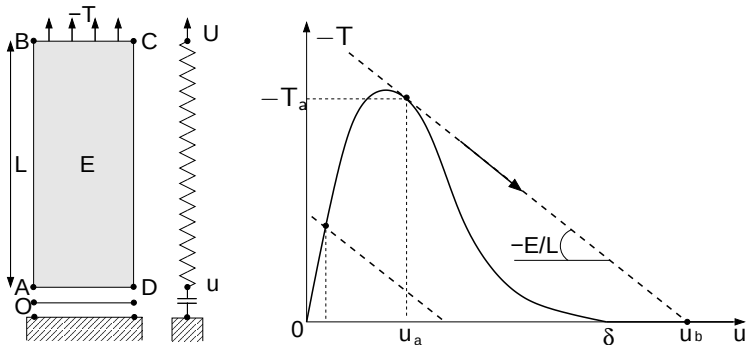

Figure 6: Uniaxial example for the occurrence of 'solution jump' during a rate-independent decohesion.

This last inequality proves that the application $\tilde{s}$ is a strict contraction from $[L^2(\Gamma_c)]^3$ to $[L^2(\Gamma_c)]^3$, if the condition

$$\lambda^2 c_1/m < 1 \tag{38}$$

is ensured. The application $\tilde{s}$ thus admits a unique fixed point, which ends the proof. ❑

This uniqueness condition can be illustrated on a simple uniaxial example which consists of an elastic bar (length L, Young modulus E) bonded to a fixed and rigid substrate by a two dimensional cohesive zone. The spatial discretization and the corresponding local behavior are plotted in Figure 6. This example was first proposed in shear by [Monerie et al., 1998] and in traction by [Chaboche et al., 2001].

Denoting by U the global displacement prescribed on BC, by T the associated stress, and by u the displacement jump across the cohesive zone, one has:

$$\mathsf{U} = \mathsf{u} - \frac{\mathsf{L}}{\mathsf{E}}\mathsf{T}. \tag{39}$$

In the present case, the cohesive law is given by (30):

$$\mathsf{T} = -\xi(\mathsf{u}). \tag{40}$$

In the local coordinates (T, u), for a given control displacement U, the local equilibrium is obtained as the intersection between the straight line

$$-\mathsf{T} = \frac{\mathsf{E}}{\mathsf{L}}(\mathsf{U} - \mathsf{u}) \tag{41}$$

defining the elastic behavior of the bar, and the softening curve $\mathsf{T} = -\xi(\mathsf{u})$ ($\mathsf{T} = 0$ for $u > \delta$). In the case of a progressive growing of U from zero, two situations can occur after the peak

stress: (i) if the ratio $\mathsf{k} = \mathsf{E}/\mathsf{L}$ (absolute value of the negative slope of the straight line) is large enough, it always exists a local equilibrium and the evolution of the decohesion is stable, (ii) if the ratio $\mathsf{k} = \mathsf{E}/\mathsf{L}$ is too small, a solution jumps from $\mathsf{u_a}$ to $\mathsf{u_b} > \mathsf{u_a}$ (Figure 6). The elastic strain energy stored in the structure is larger than the one that can be consumed at the cohesive zone, and the cohesive zone is suddenly broken.

The possibility to obtain two or tree points of local equilibrium is related to the ratio between the slope k and the larger slope of the cohesive graph in the softening part, i.e. to the ratio $|\mathsf{k}|/(\sup_{\mathsf{u}\geqslant\mathsf{u_{peak}}} |\xi'(\mathsf{u})|)$. The condition of uniqueness of a local equilibrium point is thus:

$$\frac{\sup\limits_{\mathsf{u}\geqslant\mathsf{u_{peak}}} |\partial\xi/\partial u|}{|\mathsf{E}/\mathsf{L}|} < 1. \tag{42}$$

In such an example, is it possible to identify the ratio $|\mathsf{E}/\mathsf{L}|$ to the constant of coercivity m, and $\sup|\xi'(\mathsf{u})|$ to the Lipschitz's constant c_1 of $\xi(\mathsf{u})$. If the cohesive graph has an inflexion point in its softening part, the $\sup|\xi'(\mathsf{u})|$ is reached for $\mathsf{u} > \mathsf{u_a}$ (that is, for example, the case with for Tvergaard's model), otherwise it is reached for $\mathsf{u} = \mathsf{u_a}$ (that is, for example, the case with for the model of Raous et al. [1999]).

As conclusion, the rate-independent cohesive zone models can lead to some solution jumps of quasi-static problems. The occurrence of these solutions jumps is due to the weakening part of the cohesive graph associated with the failure process, and is related to the violation of a condition of uniqueness. In one dimension, this condition states that the absolute value of the stiffness of the structure concentrated at the cohesive zone has to be larger than the absolute value of the maximal slope of the cohesive graph in its weakening portion. In other words, the 'stiffer' the cohesive law, the more sensitive to solution jump the structure; the stiffer the structure, the more insensitive to solution jump the cohesive law. For example, this condition of uniqueness can not be satisfied by a gate-like cohesive law.

In some circumstances, these solution jumps can be correlated to some instabilities, i.e. to the existence of infinite wavelength modes [Monerie, 2000, Suo et al., 1992]; and in practice, FEM simulations fail to converge. The effect of these solution jumps on the stability of extrinsic and intrinsic cohesive zone models is discussed in the following paragraph.

3.1.b The question of the equivalence and the stability between extrinsic and intrinsic cohesive zone models

The study of the stability of the cohesive zone models allows one to clarify the question of equivalence or not between cohesive zone models. We claim the following assertions:

1. for stable rectilinear crack propagation at constant speed, cohesive zone models are equivalent in terms of crack propagation if they have the same fracture toughness, and they are equivalent to the Griffith's model, (point 1)
2. this result is not ensure for other stable crack propagations, (point 2)
3. at a crack initiation or a dynamic crack branching, extrinsic and intrinsic themselves cohesive zone models, and intrinsic compared one to each other, are not equivalent, (point 3)
4. the intrinsic models are less stable than the extrinsic models. (point 4)

Points 1 and 2: the equivalence of cohesive zone models only for stable rectilinear crack propagation at constant speed. Under rectilinear steady-state propagation conditions (x_1 being the direction of propagation and $\dot{l}$ the constant crack speed), the equivalence between cohesive zone models one to each other is based on the definition of the dynamic energy release rate G [Atkinson and Eshelby, 1968, Freund, 1990, Willis, 1975]:

$$G = \lim_{\Gamma \to 0} \left\{ \frac{I(\Gamma)}{\dot{l}} \right\}, \quad \text{with} \quad I(\Gamma) = \int_{\Gamma} [\sigma \cdot n \cdot \dot{u} + (w + c)\dot{l} \cdot n_1] ds, \tag{43}$$

where Γ is an open contour which translates with the crack tip, n is here the unit output vector to Γ, w is the stress work density, t is the kinetic energy density, and $I(\Gamma)$ is the energy flux integral.

The main property of $I(\Gamma)$ in (43) is the independancy of path Γ for *steady crack growth* situations. In this case, defining Γ_{coh} as a contour embracing the cohesive zone (the zone where R^{coh} do not vanish, length d), we have by symmetry (perfect mode I):

$$\begin{aligned} G\dot{l} = I(\Gamma) = I(\Gamma_{\text{coh}}) = \int_{-d}^{0} \sigma \cdot n \cdot [\dot{u}] dx &= \int_{-d}^{0} \mathsf{R}^{coh} \cdot [\dot{u}] dx \\ &= \int_{-d}^{0} \mathsf{R}^{coh} \cdot \frac{\partial [u]}{\partial t} dx + \dot{l} \int_{0}^{\Delta} \mathsf{R}^{coh} \cdot d[u], \end{aligned} \tag{44}$$

where Δ is the critical displacement jump over which the cohesive force vanishes. Using again the fact that we consider here a steady-state propagation, the first term on the right hand side in (44) is equal to zero (constant crack speed $\dot{l}$), and we obtain:

$$G = \int_{0}^{\Delta} \mathsf{R}^{coh} \cdot d[u]. \tag{45}$$

This last equality shows that cohesive zone models are equivalent when they have the same fracture toughness ('area under the cohesive curve'): the 'shape' of the cohesive graph do not have any influence on the steady-state propagation of a rectilinear crack.

This result, due to Freund [1990], was numerically verified by Monerie et al. [1998] for mode II crack propagation. It is completed by another result by Willis [1967] which states that the model of Barenblatt [1962] and the criterion of Griffith [1920] are equivalent if $d \ll l$, i.e. if the length the cohesive zone is negligible in front of the total crack length:

$$2\gamma = \frac{\left(\dot{l}/c_2\right)^2}{\mu\pi\left(4\sqrt{1-\left(\dot{l}/c_2\right)^2} - \left[2-\left(\dot{l}/c_2\right)^2\right]^2 / \sqrt{1-\left(\dot{l}/c_1\right)^2}\right)} H^2 \left(1+\mathcal{O}\left(\frac{d}{l}\right)\right), \qquad (46)$$

where γ is the surface energy appearing in the Griffith criterion, $c_1^2 = (\lambda+2\mu)/\rho$ and $c_2^2 = \mu/\rho$ are respectively the dilatational and the shear wave speed, and H is the Barenblatt's modulus of cohesion. This result of Willis [1967], associated to the above result of Freund [1990], proves the point 1 of our list. The extensive use of the rectilinear steady-state propagation assumption yields the point 2.

Point 3: the non-equivalence of cohesive zone models at a crack initiation or a crack branching. However, Theorem 1 indicates that the 'shape' of the cohesive graph, and particularly in its weakening part, has a strong influence in two situations:

- at the crack initiation (i.e. when $l = 0$), and
- when it is no more possible to write the quantity defined by the right hand side in (45): for $[u]$ lying between $\mathsf{u_a}$ and $\mathsf{u_b}$ (see Figure 6), $[\dot{u}]$ has no more sense in (44). This case is reached when a solution jump occurs, which means that the crack no longer propagates under steady-state conditions.

The proposed uniqueness result (Theorem 1) thus indicates that different cohesive zone models may not lead to the same response in the case of crack initiation and crack branching, which explains the point 3. In particular, the difference in crack branching between extrinsic and intrinsic cohesive zone models numerically observed by Falk et al. [2001] qualitatively corroborates the result of the Theorem 1.

Point 4: extrinsic models are more stable than intrinsic models. The numerical comparative analysis of Kubair and Geubelle [2003] indicates that 'the implementation of intrinsic models is numerically less stable than that of the extrinsic models'. This conclusion can be explained a priori with the help of the simple uniaxial example in Figure 6. In the case of an extrinsic model and an intrinsic model having the same fracture toughness, the same maximum normal traction and the same critical crack opening displacement, the absolute value of the slope of the cohesive graph in its weakening part is larger for the intrinsic model than for the extrinsic one. The intrinsic models are thus more sensitive to instabilities than the extrinsic models. This situation is illustrated in Figure 7 for a linear extrinsic model and a bi-linear intrinsic model.

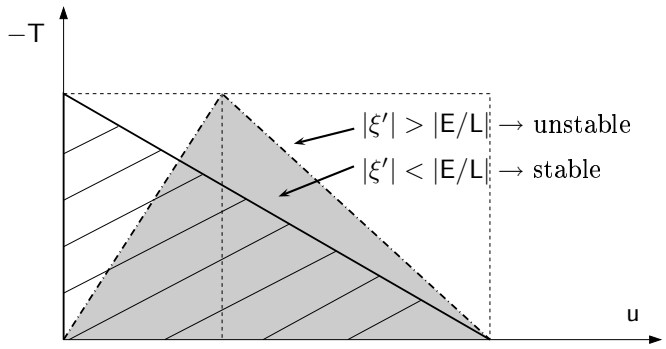

Figure 7: Comparison of a linear extrinsic model (straight line) and a bi-linear intrinsic model (dashed line) having the same fracture toughness, the same maximum normal traction, and the same critical crack opening displacement: intrinsic models is less stable than the extrinsic models (quantities $|\mathsf{E}/\mathsf{L}|$ and $|\xi'|$ correspond to equation (42)).

3.1.c The dynamical relaxation

From the numerical point of view, the aforementioned solution jumps may lead to global discontinuities and overall numerical instabilities. Various methods allow us to overcome these solution jumps [Chaboche et al., 2001]: mesh refinement, special control procedures, local control of the solution, non local formulation of the cohesive zone models, viscous regularization, and dynamic relaxation. The mesh refinement is often not acceptable for computational efficiency, in particular for brittle materials, where the small value of the critical displacement jump leads to extremely small mesh sizes. Special control procedures have to be adapted to each particular considered cases. Local controls of the solution give some fictitious equilibrium states (between u_a and u_b on Figure 6) and the energy consumed by the cohesive zone is no longer a material parameter. Volumic viscous regularizations are not physically acceptable for every classes of materials, or sometimes the viscous behavior is not clearly identified by experiments. The introduction of a surface viscous regularization is a delicate problem: (i) some efforts have to be made in order limit the rate dependency of the maximum traction (see Chaboche et al. [2001] for a complete analysis), (ii) depending on the stiffness of the structure, the energy consumed by viscosity at the cohesive zone has a minimum which is independent of the local displacement rate (Figure 8), and (iii) the energy consumed by the decohesive process can not be known a priori. The solution of a non local formulation of the cohesive zone models, first proposed by Frémond [1985] using a first gradient $\nabla\beta$ theory, introduces a new internal length, which has no clear physical meaning for homogeneous materials. All of these methods are of interest in several particular situations, but in most situations, the dynamic relaxation is the only convenient and natural solution; firstly, because, the mass is always present and secondly, because any fracture process is by

itself a dynamical process, even under quasi-static loading.

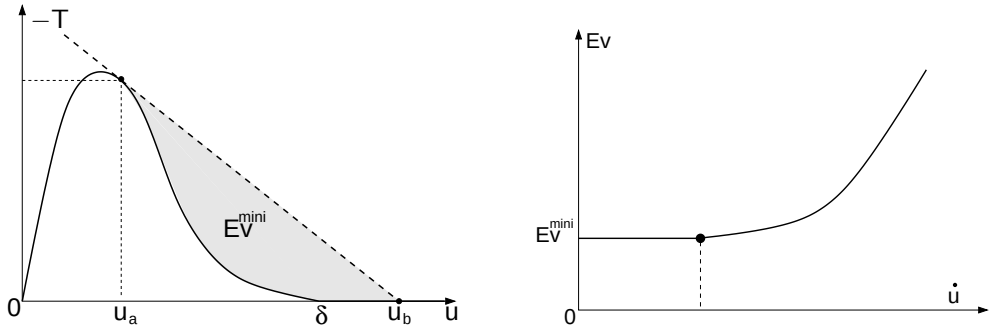

Figure 8: Viscous regularization of cohesive zone models. Left: Minimum of the energy consumed by viscosity (gray area) in order to ensure the stability of the decohesive process. Right: Evolution of the energy consumed by viscosity during a decohesive process as a function of the local velocity.

The solution retained in this paper is the dynamic relaxation. The local interpretation of this dynamic relaxation is given in Figure 9. In the dynamic version of the uniaxial example treated on section 3.1.a, the equation (41) becomes:

$$-\mathsf{T} = \frac{\mathsf{E}}{\mathsf{L}}(\mathsf{U} - \mathsf{u}) - \frac{\mathsf{M}}{\mathsf{S}}\ddot{\mathsf{u}}, \tag{47}$$

where M is the discrete mass associated to the uniaxial structure between the cohesive zone and the spring, and S is the section of the bar. If we choose an implicit time discretization scheme for the first and the second derivative of u with respect to time (47) reads as :

$$-\mathsf{T} = -\left(\frac{\mathsf{E}}{\mathsf{L}} - \frac{\mathsf{M}}{\mathsf{S}h^2}\right)\mathsf{u}_{k+1} + \left(\frac{\mathsf{E}}{\mathsf{L}}\mathsf{U} + \frac{\mathsf{M}}{\mathsf{S}h^2}(2\mathsf{u}_k - \mathsf{u}_{k-1})\right), \tag{48}$$

where h denotes the time step, the subscript k refers to the approximation of u at time $t_k = kh$. In this dynamic case, the maximum slope of the cohesive graph in its softening part $\sup|\xi'|$ has to be compared to the quantity $|\mathsf{M}/(\mathsf{S}h^2) + \mathsf{E}/\mathsf{L}|$, instead of $|\mathsf{E}/\mathsf{L}|$ in the static case. It is readily to see that when the time step vanishes, the term $|\mathsf{M}/(\mathsf{S}h^2) + \mathsf{E}/\mathsf{L}|$ becomes larger than $\sup|\xi'|$ and the decohesion is always stable. In that sense, the dynamic formulation is a relaxation of the ill-posedness of the quasi-static boundary value problem studied in section 3.1.a.

An interesting open issue is to prove an equivalent result to Theorem 1 for a time and space continuous problem.

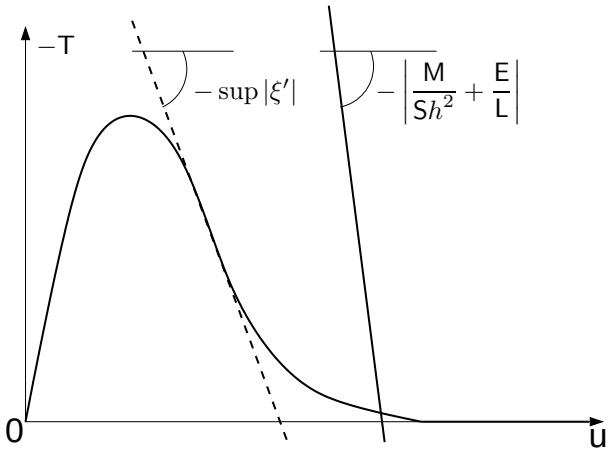

Figure 9: Local interpretation of the dynamic relaxation (quantities E/L and ξ' correspond to equation (42), and M is mass associated to the uniaxial structure depicted in Figure 6): when the time step h tends to zero, the quantity $|\mathsf{M}/(\mathsf{S}h^2)+\mathsf{E}/\mathsf{L}|$ becomes larger than $\sup|\xi'|$ and the decohesion stays always stable.

3.2 Internal length of the cohesive zone models and sensitivity to the added compliance in the intrinsic models

3.2.a Bounding the mesh size in the cohesive/volumetric finite element approach

The cohesive zone models provide a relation between a stress and a displacement (see equation (3)), or equivalently between a fracture energy and a critical stress. These models contain thus intrinsically an internal length, which plays an important role in the answer of the following two questions:

- how fine should be the mesh of the cohesive/volumetric finite element approach in order to accurately resolve the cohesive length?
- in the case of intrinsic cohesive models, does the initial slope or the stiffness of the cohesive model affect the overall elastic properties of the structure?

As we will show below, the answers to these questions require to define an upper and a lower bound for a non dimensional ratio (involving mesh size, initial slope and Young modulus of the bulk material). The bounds are often not compatible (antagonist inequality condition) leading to a non feasible set for the ratio. Theses bounds are usually given using an empirical and/or numerical way. We give here an exact lower bound based on

micromechanical arguments and we show how the upper bound can be relaxed. Furthermore, another fundamental question related to the present one is treated in Section 3.3: does the cohesive/volumetric finite element method spatially converge when the size of the volumetric elements vanishes ?

In fact, various length scales arise when using the cohesive/volumetric finite element method with intrinsic cohesive zone models. The first of these is the macroscopic length L_{struc} related to the structure. Depending on the considered problem, this length can match the size of the structure, the crack length, or the size of the remaining non cracked zone of the structure. Another physical length scale of the problem is the cohesive length L_{czm}, which can be estimated in 3D by the square root of the area over which the cohesive constitutive relation plays a role. Two other non physical length scales can also be invoked: the mesh size L_{mesh} and the length L_{int} over which the cohesive constitutive relations are solved. From the volumetric finite element point of view, it is clearly necessary to have $L_{struc} \gg L_{mesh}$ in order to obtain an accurate estimate of the stress field around the crack tip. For the cohesive surface, the same argument imposes $L_{czm} \gg L_{int}$ in order to have an accurate resolution of the cohesive zone length. The numerical simulations of Zhang and Paulino [2005] on the dynamic failure of homogeneous and functionally graded materials show that the cohesive zone length is accurately resolved for

$$L_{mesh} \leqslant \frac{1}{r} L_{czm} \quad \text{with } r \text{ about 2 or 3}, \tag{49}$$

if one identifies L_{int} to L_{mesh}. This result coincides with those of Geubelle and Baylor [1998] for intrinsic cohesive models and of Camacho and Ortiz [1996] for extrinsic cohesive models. For an homogeneous material (Young modulus E_m and Poisson coefficient ν_m), the static analysis of Rice [1968] gives the following estimate for the characteristic cohesive length scale L_{czm}:

$$L_{czm} = \frac{\pi}{8} \frac{E_m}{1-\nu_m^2} \frac{G_{Ic}}{(\mathsf{R}^{coh}_{\text{ave}})^2}, \tag{50}$$

where G_{Ic} is the mode I critical energy release rate, and $\mathsf{R}^{coh}_{\text{ave}}$ denotes the average value of R^{coh}. Using (45) for mode I crack opening, $\mathsf{R}^{coh}_{\text{ave}}$ can be linked to the cohesive peak stress $\mathsf{R}^{coh}_{\text{max}}$ by:

$$\mathsf{R}^{coh}_{\text{ave}} = \frac{1}{\Delta} \int_0^{\Delta} \mathsf{R}^{coh}_N du_N = \zeta \mathsf{R}^{coh}_{\text{max}}, \quad \zeta \leqslant 1, \tag{51}$$

where ζ depends on the cohesive zone model: for a Barenblatt type cohesive zone model (constant traction-separation relation) $\zeta = 1$; for the model proposed in Section 2.3.b, $\zeta = (9 - 4ln4)/6 \simeq 0.57$; for the cohesive model of Tvergaard [1990], $\zeta = 27/48 \simeq 0.56$; and for the extrinsic cohesive model of Camacho and Ortiz [1996], $\zeta = 1/2$. Combining (49), (50) and (51), one obtains:

$$L_{mesh} \leqslant \frac{1}{r\zeta^2} \frac{\pi}{8} \frac{E_m}{1-\nu_m^2} \frac{G_{Ic}}{(\mathsf{R}^{coh}_{\text{max}})^2} \quad \text{with } r \simeq \text{2-3 and } \zeta \leqslant 1. \tag{52}$$

However, these spatial resolution considerations have to be completed by mechanical considerations on the overall compliance added by intrinsic cohesive models. The initial slope of intrinsic cohesive models as well as the penalty parameter (for the fracture of homogeneous materials, for example) can be understood as a mechanical parameter defining the stiffness of an interface (or interphase between two phases, for example). In the case of homogeneous or functionally graded materials, this initial slope, denoted here C_N, must satisfy the following condition: the wave speed in the material must not be affected by the cohesive zone model or, equivalently, such that the overall stiffness of the material must not be affected by the stiffness of the cohesive zone model. The numerical study of Espinosa and Zavattieri [2003] shows that these conditions are satisfied when

$$C_N \geqslant \tilde{r}\frac{E_m}{L_{mesh}} \quad \text{with } \tilde{r} \simeq 10. \tag{53}$$

To fix ideas on the compatibility between the conditions (52) and (53), let us consider a perfect elastic brittle cohesive zone model, for which $\zeta = 1/2$ and $(\mathsf{R}_{\max}^{coh})^2 = 2C_N G_{Ic}$. The conditions (52) and (53) then rewrite:

$$\tilde{r} \leqslant \frac{C_N L_{mesh}}{E_m} \leqslant \frac{1}{r}\frac{\pi}{4}\frac{1}{1-\nu_m^2}. \tag{54}$$

It is readily seen that these lower and upper empirical bounds on $C_N L_{mesh}/E_m$ do not lead to a feasible choice for C_N: the lower bound is about 10 and the upper bound is about 0.3. In other words, it is not possible to accurately resolve the cohesive zone without affecting the overall stiffness of the solid. Analyzing another type of ratio dedicated to extrinsic cohesive models, Falk et al. [2001] obtain the same conclusion by considering the cohesive law of Camacho and Ortiz [1996].

Two comments may be made on this paradox:

a) Firstly, the above considerations for the upper bound on $C_N L_{mesh}/E_m$ hold if L_{int} is identified to L_{mesh}. The length L_{int} is almost never considered by authors developing cohesive zone modeling. In practice, if one uses linear volumetric finite elements, and if the nodes dedicated to the integration of the surface constitutive relations have the same position to those of the volumetric finite elements, one has $L_{int} = L_{mesh}$, and the two quantities can be identified one to each other. A contrario, if one uses higher order volumetric finite elements, or if one uses more nodes for the integration of the surface constitutive relations than for the bulk constitutive relations, one has $L_{int} = (1/p)L_{mesh}$, with $p \geqslant 1$. In this last case, the right member of (54) is multiplied by $p \geqslant 1$. This remark, associated to the fact that the estimate (50) is obtained by a static analysis, indicates that the upper bound on $C_N L_{mesh}/E_m$ can be relaxed for dynamic cracks by incorporating numerous cohesive nodes along the mesh-cell edges.

b) Secondly, the value $\tilde{r} \simeq 10$ of the lower bound was obtained numerically by Espinosa and Zavattieri [2003] on a given situation with a particular type of numerical treatment

and finite elements. This value has to be confirmed in the general case. This problem is studied in the next paragraph.

3.2.b A criterion for 'invisible' cohesive zones

The cohesive/volumetric finite element method tends to add some compliance in the structure, even in the elastic regime of the cohesive zone (i.e. before the beginning of the surface damage). Quantifying and limiting this spurious compliance is an important feature for the practical use of the cohesive/volumetric finite element approach.

In order to answer to this question, we investigate a purely elastic model without damage: we determine, with the help of micromechanical arguments, the effect of this added compliance on the overall elastic moduli. The case of a mesh with homogeneous elastic properties is considered. The studied microstructure consists in penny shaped elastic inclusions randomly distributed in space and in orientation embedded into an homogeneous elastic matrix. The fourth-order stiffness tensor of the matrix, respectively the inclusions, is denoted by $\mathbb{C}_m$, respectively by $\mathbb{C}_i$. Since the considered matrix is here a classical elastic medium, $\mathbb{C}_m$ is written as:

$$\mathbb{C}_m = 3k_m\mathbb{J} + 2\mu_m\mathbb{K}, \tag{55}$$

where k_m and μ_m are respectively the bulk modulus and the shear modulus of the matrix. The tensors $\mathbb{J}$ and $\mathbb{K}$ define the standard base of the fourth-order isotropic tensor: $\mathbb{J} = \frac{1}{3}i\otimes i$, $\mathbb{K} = \mathbb{I} - \mathbb{J}$, with i the identity of the second-order tensors and $\mathbb{I}^{kl}_{ij} = \frac{1}{2}(\delta_{ik}\delta_{jl} + \delta_{il}\delta_{jk})$ the identity of the fourth-order tensors.

The elastic tensor of the inclusions $\mathbb{C}_i$ is here defined thanks to a small length parameter, e. This parameter stands for the thickness of an equivalent domain represented by a cohesive zone model (without thickness), and should then vanish. We claim that $\mathbb{C}_i$ is given by the following relation:

$$\mathbb{C}_i = e\tilde{\mathbb{C}}, \quad \text{with} \quad \tilde{\mathbb{C}} = C_N\mathbb{E}_l + C_T\mathbb{K}_l, \tag{56}$$

where the tensors $\mathbb{E}_l$ and $\mathbb{K}_l$ are respectively the uniaxial strain along the normal n to the interface and the longitudinal shear strain:

$$\mathbb{E}_l = n\otimes n\otimes n\otimes n \tag{57}$$

$$\mathbb{K}_l = 2\left(j_s\otimes j_s + j_t\otimes j_t\right) \text{ where } j_\alpha = n\otimes_s\alpha. \tag{58}$$

The vectors s and t define an orthonormal basis of the plane tangent to the cohesive zone, and $n\otimes_s\alpha = (n\otimes\alpha + \alpha\otimes n)/2$. The relation (56) can be proved using the equations (121) and (4) of the ECZM in the elastic case, i.e.for $\beta = 1$. In this particular case, the stress

tensor across a cohesive zone of normal n reads:

$$\begin{aligned}
\sigma &= \mathsf{R}^{coh} \otimes_s n \\
&= \left(\left(C_N n \otimes n + C_T \frac{u_T \otimes u_T}{\|u_T\|^2} \right) \cdot [u] \right) \otimes_s n \\
&= (C_N u_N n + C_T u_T) \otimes_s n \\
&= C_N u_N n \otimes_s n + C_T u_T \otimes_s n \\
&= C_N u_N \mathbb{E}_l : (n \otimes_s n) + C_T \mathbb{K}_l : (u_T \otimes_s n) \\
&= (C_N \mathbb{E}_l + C_T \mathbb{K}_l) : (u_N n \otimes_s n + u_T \otimes_s n) \\
&= (C_N \mathbb{E}_l + C_T \mathbb{K}_l) : ([u] \otimes_s n). \qquad (59)
\end{aligned}$$

As underlined by Michel and Suquet [1994], the strain across a small layer of thickness e can be approached by:

$$\varepsilon(u) \simeq \frac{[u] \otimes_s n}{e}. \qquad (60)$$

Combining equations (60) and (59) yields the property (56).

The overall elastic tensor $\mathbb{C}^{\mathsf{hom}}$ of the microstructure studied in this paragraph can be sized with the help of Hashin and Shtrikman [1963]-like estimates:

$$\mathbb{C}^{\mathsf{hom}}\left(\mathbb{C}^0\right) = \left[f \left[\mathbb{C}^*\left(\mathbb{C}^0\right) + \mathbb{C}_i \right]^{-1} + (1-f) \left[\mathbb{C}^*\left(\mathbb{C}^0\right) + \mathbb{C}_m \right]^{-1} \right]^{-1} - \mathbb{C}^*\left(\mathbb{C}^0\right) \qquad (61)$$

where the real value $f \in [0,1]$ is the volumic fraction of inclusions and the tensor function $\mathbb{C}^*\left(\mathbb{C}^0\right)$ is by:

$$\mathbb{C}^*\left(\mathbb{C}^0\right) = \mathbb{C}^0 : \left[\mathbb{S}\left(\mathbb{C}^0\right) - \mathbb{I} \right]. \qquad (62)$$

The tensor $\mathbb{S}\left(\mathbb{C}^0\right)$ is the Eshelby tensor related to an inclusion embedded in an infinite medium of elastic tensor $\mathbb{C}^0$. The volumic fraction f may be defined by the product eZ (where Z is a density parameter). For the present case of penny shaped inclusions, e tends to zero and the Eshelby tensor has the following simple form [Mura, 1982]:

$$\mathbb{S}\left(\mathbb{C}^0\right) = \mathbb{E}_l + \mathbb{K}_l. \qquad (63)$$

Various bounds and estimates for $\mathbb{C}^{\mathsf{hom}}$ can be derived from (61) according to the choice of the reference medium $\mathbb{C}^0$. When e vanishes, (i.e. $\mathbb{C}_i = e\tilde{\mathbb{C}} \to 0$, and $f = eZ \to 0$), the Hashin and Shtrickman upper bound ($\mathbb{C}^0 = \mathbb{C}_m$), the Mori and Tanaka estimate ($\mathbb{C}^0 = \mathbb{C}_m$), and the self consistent estimate ($\mathbb{C}^0 = \mathbb{C}^{\mathsf{hom}}$) are equal and give the trivial result: $\mathbb{C}^{\mathsf{hom}} = \mathbb{C}_m$. However, the Hashin and Shtrickman lower bound leads to:

$$\mathbb{C}^{\mathsf{HS}^-} = \mathbb{C}^{\mathsf{hom}}\left(\mathbb{C}_i\right) = \left(Z\mathbb{S} : \tilde{\mathbb{C}}^{-1} + \mathbb{C}_m^{-1} \right)^{-1}. \qquad (64)$$

Using (63) and (56), one finds

$$\mathbb{S} : \tilde{\mathbb{C}}^{-1} = \frac{1}{C_N}\mathbb{E}_l + \frac{1}{C_T}\mathbb{K}_l. \tag{65}$$

Since we have interest in inclusions randomly distributed in space and in orientation, the overall elastic tensor $\mathbb{C}^{\mathsf{hom}}$ has to be isotropic, and from this point of view, the quantity $\mathbb{S} : \tilde{\mathbb{C}}^{-1}$ has to be averaged over all possible orientations. This particular average reads [Gatt et al., 2005]:

$$\left\langle \mathbb{S} : \tilde{\mathbb{C}}^{-1} \right\rangle_{\circlearrowleft} = P_{\mathbb{JK}}\left(\mathbb{S} : \tilde{\mathbb{C}}^{-1}\right) \tag{66}$$

where $P_{\mathbb{JK}}(A)$ denotes the projection of any fourth order tensor A on the base $\{\mathbb{J}, \mathbb{K}\}$ and $\langle A \rangle_{\circlearrowleft}$ is th average over all the possible orientations of any tensor A. This last quantity is equal to

$$\left\langle \mathbb{S} : \tilde{\mathbb{C}}^{-1} \right\rangle_{\circlearrowleft} = \frac{1}{3C_N}\mathbb{J} + \frac{2}{5}\left(\frac{1}{3C_N} + \frac{1}{C_T}\right)\mathbb{K}. \tag{67}$$

Writing $\mathbb{C}^{\mathsf{HS}^-}$ in the form

$$\mathbb{C}^{\mathsf{HS}^-} = 3k^{\mathsf{HS}^-}\mathbb{J} + 2\mu^{\mathsf{HS}^-}\mathbb{K} \tag{68}$$

where k^{HS^-} and μ^{HS^-} are respectively the overall bulk and shear moduli, and using equation (64), one obtains after some algebra:

$$\frac{k^{\mathsf{HS}^-}}{k_m} = \frac{x}{1-x} \text{ with } x = \frac{C_N}{k_m Z}, \tag{69}$$

$$\frac{\mu^{\mathsf{HS}^-}}{\mu_m} = \frac{y}{1-y} \text{ with } y = \frac{15C_N C_T}{4\mu_m(C_T + 3C_N)Z}. \tag{70}$$

Combining k^{HS^-} and μ^{HS^-} gives the following lower bound for the overall Young modulus:

$$\frac{E^{\mathsf{HS}^-}}{E_m} = \frac{\xi}{1+\xi}, \text{ where } \xi = \frac{5}{1 + \frac{4}{3}\frac{C_N}{C_T}}\frac{C_N}{E_m Z}, \tag{71}$$

where E_m being the Young modulus of the matrix.

At this stage, the comparison of various cases of cohesive zone models is an interesting issue. Firstly, for 'no shear' CZM (i.e. CZM involving no tangential reaction), the condition

$$C_T = 0 \text{ gives } \xi = 0, \tag{72}$$

and the initial normal elasticity of the cohesive zone have to be infinite in order to obtain a non vanishing overall elasticity for the structure. Second, for 'no sliding' CZM (i.e. CZM involving no tangential sliding), the condition

$$C_T \to \infty \text{ gives } \xi = \frac{5C_N}{E_m Z}. \tag{73}$$

Third, for the frequent case of equal normal and tangential elasticity, the condition

$$C_N = C_T \text{ gives } \xi = \frac{15}{7}\frac{C_N}{E_m Z}. \tag{74}$$

In what follows, the relation $C_N = C_T$ is assumed. The question of estimating the density parameter Z depends on the type of mesh which is used. In order to illustrate the accuracy of the lower bound (71) and the relation (74), we consider the 2D case of a square meshed with regular squares divided in four equal isosceles triangles. We denote by L_{mesh} the length of the larger side of each triangles, by p the number of meshes by side of the square, by l the total length of cohesive zone (total length of boundaries between meshes), and by N the number of meshes. For non vanishing thickness e of cohesive zone, the volumic fraction f reads:

$$f = \frac{le}{le + (L_{mesh}^2/4)N}, \tag{75}$$

and when $e \to 0$, the relation $f = Ze$ gives the limit case:

$$Z = \frac{4l}{L_{mesh}^2 N}. \tag{76}$$

The total length of cohesive zone l is related to parameters L_{mesh} and p:

$$l = 2\sqrt{2}L_{mesh}p^2 + 2p(p-1)L_{mesh}. \tag{77}$$

For large meshes (i.e. when $p \to \infty$), one finds:

$$Z = \frac{2(1+\sqrt{2})}{L_{mesh}}. \tag{78}$$

Putting this last equation in (71), the following lower bound holds for this type of meshes:

$$\frac{E^{\text{HS}^-}}{E_m} = \frac{\xi}{1+\xi}, \text{ where } \xi = \frac{5/(1+\sqrt{2})}{2\left(1+\frac{4}{3}\frac{C_N}{C_T}\right)}\frac{C_N L_{mesh}}{E_m}. \tag{79}$$

The accuracy of this lower bound is illustrated on Figure 10 where the overall Young modulus of an elastic structure including elastic cohesive zone models at each finite elements boundary is plotted for various parameters ξ. The range of parameter ξ is about $[0, 40]$ with $C_N/C_T \in [1/3, 10/3]$ and $C_N L_{mesh}/E_m \in [7 \times 10^{-3}, 51]$.

For the particular case $C_N = C_T$, the following criterion can be written:

$$\frac{C_N L_{mesh}}{E_m} \geqslant 21 \Longrightarrow \frac{E^{\text{HS}^-}}{E_m} \geqslant 0.9. \tag{80}$$

This criterion being related to the lower bound of the overall stiffness of the solid, it is noteworthy that, in practice, the numerical-based criterion of Espinosa and Zavattieri [2003] should be relevant for any type of situations, even those very far from what they studied.

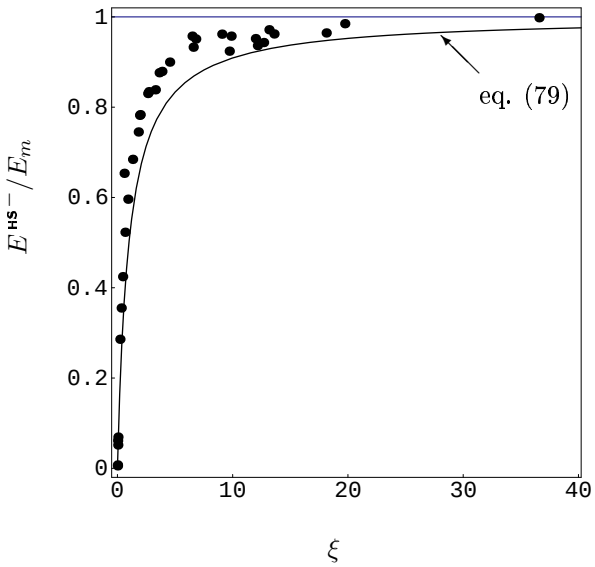

Figure 10: Overall Young modulus of an elastic structure including elastic cohesive zone models at each finite elements boundary for various parameters ξ (see equation (79)): numerical results (points) and lower bound (79).

3.3 Mesh and time-step dependencies

3.3.a Illustration of the mesh independence of the overall fracture properties

The question of the spatial convergence of the cohesive/volumetric finite element method is often debated in the literature (see, for example, the recent review of de Borst et al. [2006]). The work of Tijssens et al. [2000] has shown for the first time that this approach suffers from a certain mesh bias, and that the initial mesh design can drastically affect the final crack path. From this point of view, the so-called cohesive segments method was developed by exploiting the partition-of-unity property in order to avoid this problem Remmers et al. [2003]. But, from the point of view of the spatial convergence the conclusion is quite different. First, the work of Papoulia et al. [2006] proves the spatial convergence of crack nucleation within the cohesive/volumetric finite element framework using extrinsic cohesive models and a so-called pinwheel-based mesh having the isoparametric property (this property states that it is possible to found a broken line based on mesh-cell edges that tends to any given curve on the computational domain when the grid size tends to zero). Second, the study proposed here illustrates the fact that the cohesive/volumetric finite element method using intrinsic models can lead to mesh independent overall fracture properties since the finite element discretization error is acceptable and the initial cohesive stiffness is calibrated using the proposed criterion (80).

In this illustration, the representative volume element considered is a square with length $L = 10\mu m$ under plane strain hypothesis (section $\mathsf{S} = 10^{-5}m^2$). The material is assumed to be Neo-Hookean brittle: Young modulus $E_m = 135GPa$, Poisson coefficient $\nu_m = 0.32$, critical energy release rate $G_{Ic} = 0.5J/m^2$, and density equal to $7800kg/m^3$. The used cohesive law is the one given on section 2.3.b with $C_N = C_T$, a low friction coefficient $\mu = 0.05$, and no soft coupling between cohesion and friction $\kappa = 1$. Velocity boundary conditions are imposed along vertical faces ($V = 2m/s$), and an initial crack is inserted at the center of the structure and perpendicular to the loading direction.

The mesh convergence is studied through the macroscopic fracture energy $\mathcal{E}$, composed by the dissipated energies during the fracture process, as a function of the mesh size L_{mesh}. The finite element discretization is based on linear displacement triangular elements that are arranged in a "crossed-triangle" quadrilateral pattern and four mesh sizes considered are : $0.2\mu m$ (10000 meshes), $0.25\mu m$ (6400 meshes), $0.33\mu m$ (3600 meshes) and $0.5\mu m$ (1600 meshes). The initial cohesive stiffness C_N is adapted for each mesh in order to verify the criterion (80): $C_N L_{mesh}/E_m \geqslant 21$.

The Figure 11 shows the rupture features of the mesh sizes considered. Although the cracks paths are noticeably different, the macroscopic fracture energy $\mathcal{E}$ is constant for each mesh size (see Table 1). This result demonstrates the mesh size independence of the overall fracture properties of the two following conditions are satisfied:

a) the mesh size is enough small such that the finite element discretization error is acceptable and,

b) the initial cohesive stiffness is well calibrated using the criterion (80).

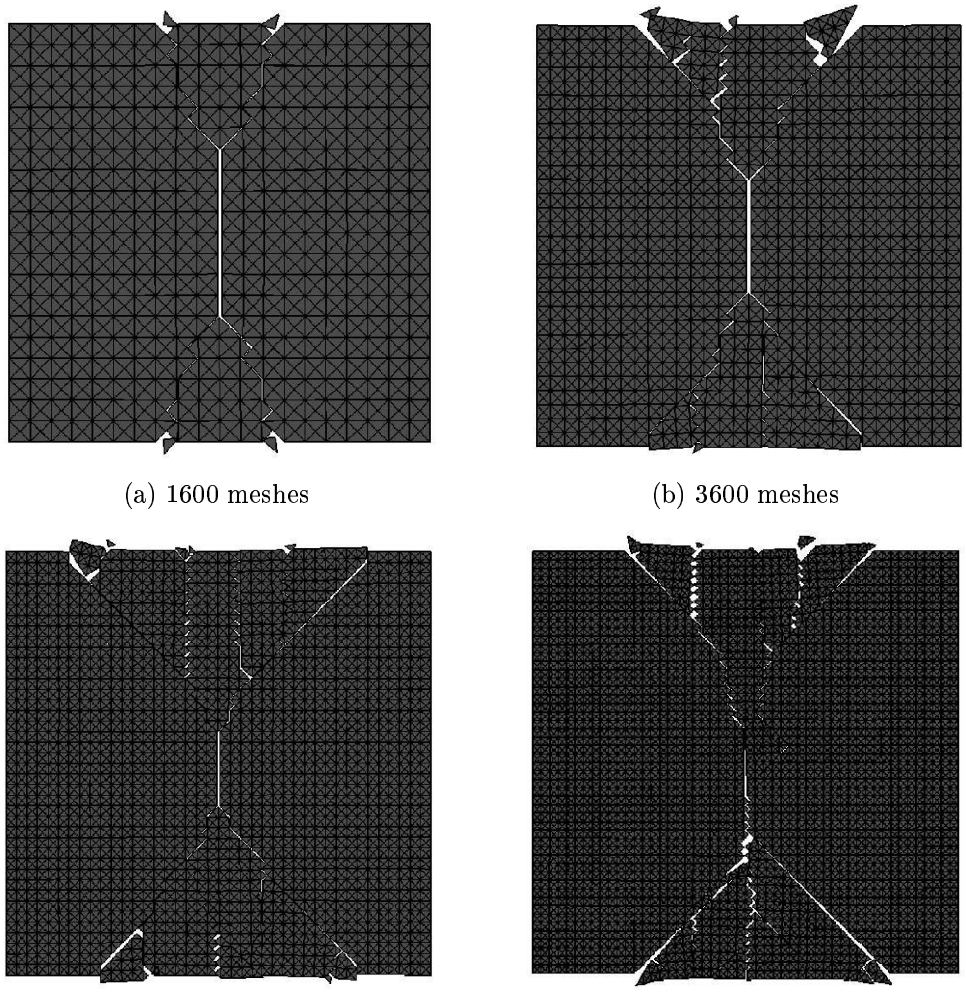

(a) 1600 meshes (b) 3600 meshes

(c) 6400 meshes (d) 10000 meshes

Figure 11: Rupture features for various meshes using an adapted initial cohesive stiffness with respect to the criterion (80): $C_N L_{mesh}/E_m \geqslant 21$.

L_{mesh}/L	5.0×10^{-2}	3.3×10^{-2}	2.5×10^{-2}	2.0×10^{-2}
$\mathcal{E}/(G_{Ic}\mathsf{S})$	21.62	21.80	22.20	22.20

Table 1: Normalized macroscopic fracture energy in function of the non dimensional mesh size for an adapted initial cohesive stiffness using the obtained criterion (80): $C_N L_{mesh}/E_m \geqslant 21$.

4 Non Smooth Dynamics formulation

This section aims at introducing a particular formulation of the Dynamics, the so–called *Nonsmooth Dynamics*. Two kinds of nonsmoothness are considered: the eventual non–differentiability of the dynamics with respect to time, more precisely of the state variables and the multi–valued, and then nonsmooth, description of the constitutive laws. As we have already seen in the formulation of the ECZM (1)–(3), Nonsmooth Analysis, Convex Analysis and Set-valued Analysis [Hiriart-Urruty and Lemaréchal, 1993] play an important role in our setting. The term "nonsmooth" refers firstly to all the mathematical and mechanical background allowing us to deal with some extended kinds of laws. For the nonsmoothness in time, the occurrence of velocity jumps is a well known feature of the second order dynamics with unilateral constraints on the position even with continuum media. This fact leads us to take some precautions when the dynamics is formulated. Especially, the notion of second order derivative of the position has no usual sense when the dynamics is nonsmooth. Measure Theory on the real line will help us to adequately formulate our problem.

4.1 The smooth equations of motion

In this section, the smooth equations of motion of a collection of N continuum media are introduced in a quite usual setting. The continuum medium is identified at time $t \in [0, T]$ by its volume in $\mathbb{R}^d$. The integer $d = 1, 2, 3$ denotes the space dimension, of interior

$$\Omega^i(t) \subset \mathbb{R}^d, i \in \{1, \ldots, N\}$$

and boundary $\partial\Omega^i(t)$. If Ω^i is a deformable continuum medium, the equations of motion are introduced through the principle of virtual powers in a finite strain Lagrangian setting permitting a space-discretization based on a conventional finite element method. If Ω^i is assumed to be a rigid body, the equation of motion will be described by a finite set of coordinates. In both cases, possibly after a space-discretization, the equations of motion will be formulated and treated in a single finite-dimensional framework.

A material particle is described by its position, X in a reference frame at $t = 0$ and by its current position $x = \varphi(X, t)$ at time t. For a Lagrangian description, we also assume we know at least formally the function $X = \psi(x, t)$. The displacement is defined by $u(x, t) = x - X = x - \psi(x, t)$ and the velocity and the acceleration are denoted by $\dot{u}$ and $\ddot{u}$. Most of the Lagrangian variables expressed in terms of X are denoted by capitals letters, for instance,

$U(X,t)$ for the displacement, and denoted by lower case for the associated Eulerian variables, in this case $u(x,t)$. This convention can be summarized by $u(x,t) = u(\varphi(X,t),t) = U(X,t)$.

Principle of virtual powers in continuum mechanics. Starting from the equation of motion in Eulerian coordinates,

$$\operatorname{div}\sigma(x,t) + \rho(x,t)b(x,t) = \rho(x,t)\ddot{u}(x,t), \forall x \in \Omega^i(t), \tag{81}$$

where $\sigma(x,t)$ is the Cauchy stress tensor and $b(x,t)$ is the density of body forces, the principle of virtual power states that

$$\int_{\Omega^i(t)} (\ddot{u}(x,t) - b(x,t))\hat{v}(x,t)\, dm(x,t) = \int_{\Omega^i(t)} \operatorname{div}\sigma(x,t)\hat{v}(x,t)\, d\omega(x,t), \tag{82}$$

for all virtual velocities denoted by $\hat{v}(x,t)$. The measure $d\omega(x,t)$ denotes the Lebesgue measure in $\mathbb{R}^d$ at x and the measure $dm(x,t) = \rho(x,t)\, d\omega(x,t)$ is the mass measure. With the help of the Green formulas, the principle of virtual power is usually reformulated as

$$\begin{aligned}\int_{\Omega^i(t)} (\ddot{u}(x,t) - b(x,t))\hat{v}(x,t)\, dm(x,t) = &- \int_{\Omega^i(t)} \sigma(x,t) : \nabla\hat{v}(x,t)\, d\omega(x,t) \\ &+ \int_{\partial\Omega^i_F(t)} t(x,t)\hat{v}(x,t)\, ds(x,t) + \int_{\Gamma^i_c(t)} r(x,t)\hat{v}(x,t)\, ds(x,t)\end{aligned} \tag{83}$$

where $A : B = A_{ij}B^{ij}$ is the double contracted tensor product, and $t(x,t) = \sigma(x,t).n(x,t)$ is the applied forces on the boundary of outward normal n and $r(x,t)$ the reaction forces due to the cohesive interface. The measure $ds(x,t)$ is the Lebesgue measure at $x \in \partial\Omega^i$. The symmetry of the Cauchy stress tensor in absence of density of momentum allows one to introduce the symmetric deformation rate tensor,

$$D(x,t) = \frac{1}{2}(\nabla^T v(x,t) + \nabla v(x,t)) \tag{84}$$

leading to the standard expression of the virtual power of the internal forces of cohesion

$$\hat{\mathcal{P}}_{int} = -\int_{\Omega^i(t)} \sigma(x,t) : \nabla\hat{v}(x,t)\, d\omega(x,t) = -\int_{\Omega^i(t)} \sigma(x,t) : \hat{D}(x,t)\, d\omega(x,t) \tag{85}$$

In order to formulate the principle of virtual power in a total Lagrangian framework, the second Piola–Kirchhoff tensor,

$$S(X,t) = F^{-1}\det(F)\sigma^T F^{-T}$$

is introduced, where $F = \dfrac{\partial x}{\partial X} = \dfrac{\partial\varphi(X,t)}{\partial X}$ is the deformation gradient. The virtual power of the internal forces is then rewritten, as

$$\hat{\mathcal{P}}_{int} = -\int_{\Omega^i(t)} \sigma(x,t) : \nabla\hat{v}(x,t)\, d\omega(x,t) = -\int_{\Omega^i(0)} S(X,t) : \hat{L}(X,t)\, d\Omega(X,0) \tag{86}$$

where $L = \dot{F}$. Finally, the principle of virtual power in a total finite strain Lagrangian framework in terms of the convected Lagrangian variable X, is

$$\int_{\Omega^i(0)} (\ddot{U}(X,t) - B(X,t))\hat{V}(X,t)\, dM(X,0) = -\int_{\Omega^i(0)} S(X,t) : \hat{L}(X,t)\, d\Omega(X,0) + \int_{\partial\Omega^i(0)} T(X,t)\hat{V}(X,t)\, dS(X,t) + \int_{\Gamma_c^i(0)} R(X,t)\hat{V}(X,t)\, dS(X,t) \tag{87}$$

where the applied forces laws on the boundary satisfies $T(X,t) = S(X,t).F^T(X,t).N(X,t)$ and $R(X,t) = S(X,t).F^T(X,t).N(X,t)$. It is noteworthy that the interactions between bodies that are taken into account in this model are only given by the forces through the cohesive interface with unilateral contact and friction.

For the constitutive material laws, a large panel of models can be taken into account in this framework and in the numerical applications. The formulation of the constitutive laws is based on the standard thermodynamics of irreversible processes [Germain et al., 1983] or based on a variational formulation of incremental stress-strain relation deriving from a pseudo elastic potential [Ortiz and Stainier, 1999]. When the behavior is not explicitly mentioned in the further numerical experiments, the bulk response of the material is supposed to be linear elastic, that is

$$S(X,t) = K(X,T) : E(X,t), \tag{88}$$

where E is the Green-Lagrange strain tensor,

$$E(X,t) = \frac{1}{2}(F^T(X,t)F(X,t) - I(X,t)), \tag{89}$$

the tensor I is the identity tensor and $K(X,T)$ is the fourth order tensor of elastic properties.

The finite element discretization is conventional and is based on this principle of virtual power in this total Lagrangian framework. Choosing some isoparametric element leads to the following approximation

$$U(X,t) = \sum_h N^h(X,t)U_h(t), \quad \dot{u}(X,t) = \sum_h N^h(X,t)\dot{U}_h(t), \quad \ddot{U}(X,t) = \sum_h N^h(X,t)\ddot{U}_h(t), \tag{90}$$

where N^h are the shape functions and U_h the finite set of displacement at nodes. Substituting this approximation into the principle of virtual power and simplifying with respect to the virtual field yields a space-discretized equation of motion of the form

$$M(U_h)\ddot{U}_h + F(t, U_h, \dot{U}_h) = R, \tag{91}$$

where $M(U_h)$ is the consistent or lumped mass matrix, the vector $F(t, U_h, \dot{U}_h)$ collects the internal and external discretized forces and R are the discretized forces due to the cohesive zone model.

Principle of virtual powers in rigid body mechanics. In rigid body mechanics, it is assumed that the power of the cohesion internal forces vanishes for a rigid motion given by the following set of virtual velocity field,

$$\mathcal{V} = \{\hat{v}(x,t) = \hat{v}_O(t) + \hat{\omega}(t) \times (x - x_O), \forall x \in \Omega^i(t)\}, \tag{92}$$

where O is a geometrical point fixed with respect to the body, x_O is the position of this point $v_O(t)$ is its velocity, and $\omega(t)$ the angular velocity of the body at O. This assumption yields

$$\int_{\Omega^i(t)} (\ddot{u}(x,t) - b(x,t))\hat{v}(x,t)\, dm(x,t) = \int_{\partial\Omega^i(t)} t(x,t)\hat{v}(x,t)\, ds(x,t), \qquad \forall \hat{v}(x,t) \in \mathcal{V} \tag{93}$$

The equation of motion can be derived choosing a particular virtual velocity as:

$$\begin{cases} \dfrac{d}{dt}\displaystyle\int_{\Omega^i(t)} \dot{u}(x,t)\, dm(x,t) = \int_{\Omega^i(t)} b(x,t)\, dm(x,t) + \int_{\partial\Omega^i(t)} t(x,t)\, ds(x,t), \\ \dfrac{d}{dt}\displaystyle\int_{\Omega^i(t)} (x - x_O) \times \dot{u}(x,t)\, dm(x,t) = \int_{\Omega^i(t)} (x - x_O) \times g(x,t)\, dm(x,t) \\ \qquad\qquad + \displaystyle\int_{\partial\Omega^i(t)} (x - x_O) \times t(x,t)\, ds(x,t). \end{cases} \tag{94}$$

Various descriptions of the equations of motion of a rigid body can be deduced from the principle of virtual power choosing particular kinematics. Without going into further details, the Newton-Euler formulation can be chosen to write the kinematics with respect to the center of mass G_i of the body Ω^i in Eulerian coordinates:

$$\begin{cases} \dot{u}(x,t) = v_{G_i}(t) + \omega_i(t) \times (x - x_{G_i}), \\ \ddot{u}(x,t) = \dot{v}_{G_i}(t) + \dot{\omega}_i(t) \times (x - x_{G_i}) + \omega_i(t) \times (\omega_i(t) \times (x - x_{G_i})). \end{cases} \tag{95}$$

Substituting (95) into the equations of motion (94) yields the well-known Newton-Euler equations,

$$\begin{bmatrix} M & 0 \\ 0 & I \end{bmatrix} \frac{d}{dt} \begin{bmatrix} v_{G_i}(t) \\ \omega_i(t) \end{bmatrix} + \begin{bmatrix} 0 \\ \omega_i(t) \times I\omega_i(t) \end{bmatrix} = \begin{bmatrix} f_{ext}(t) \\ m_{ext}(t) \end{bmatrix}, \tag{96}$$

where

$$\begin{aligned} M &= \int_{\Omega^i(t)} dm(x,t) = \int_{\Omega^i(0)} dM(X,0), \\ I &= \int_{\Omega^i(t)} (x - x_{G_i})^T (x - x_{G_i})\, dm(x,t), = \int_{\Omega^i(0)} (X - X_{G_i})^T (X - X_{G_i})\, dM(X,0), \\ f_{ext}(t) &= \int_{\Omega^i(t)} b(x,t)\, dm(x,t) + \int_{\partial\Omega^i(t)} t(x,t)\, ds(x,t), \\ m_{ext}(t) &= \int_{\Omega^i(t)} (x - x_{G_i}) \times b(x,t)\, dm(x,t) + \int_{\partial\Omega^i(t)} (x - x_{G_i}) \times t(x,t)\, ds(x,t). \end{aligned} \tag{97}$$

Usually, a second order form of the dynamics is obtained with the help of the following parametrization of the vector ω_i,

$$\omega_i(t) = D_i(\Psi, t)\dot{\Psi}_i(t), \tag{98}$$

where $D(\Psi, t)$ is supposed to be a diffeomorphism. For a collection of N rigid bodies, a usual way is to introduce a set a generalized coordinates z such that

$$z = \left[[\, x_{G_i},\, \Psi_i \,]_{i\in\{1\ldots N\}} \right]^T \tag{99}$$

assuming that the positions and the orientations of the bodies are uniquely determined by z. With this variable, after some algebraic manipulations, the equations of motion can be written as:

$$M(z)\ddot{z} + F(t, z, \dot{z}) = r \tag{100}$$

It is noteworthy that this formulation allows us to add some internal forces between bodies expressed in terms of the generalized coordinates z.

Clearly, the equations of motion can also be obtained straightforwardly thanks to the Lagrangian formalism postulating the existence of the Lagrangian of the system,

$$L(z, \dot{z}) = T(z, \dot{z}) - V(z),$$

composed of the kinetic energy,

$$T(z, \dot{z}) = \frac{1}{2}\dot{z}^T M(z)\dot{z}$$

and the potential energy of the system, $V(z)$. The Lagrange's equations can be written as

$$\frac{d}{dt}\left(\frac{\partial L(z,\dot{z})}{\partial \dot{z}_i}\right) - \frac{\partial L(z,\dot{z})}{\partial z_i} = Q_i(z,t), \quad i \in \{1\ldots n\}, \tag{101}$$

where the vector $Q(z,t), \in I\!R^n$ denotes the set of generalized forces. With some standard algebraic manipulations, the Lagrange equations (101) can be put in a more usual form:

$$M(z)\frac{d\dot{z}}{dt} + N(z,\dot{z}) = Q(z,t) - \nabla_z V(z) \tag{102}$$

where the vector $N(z,\dot{z}) = \left[\frac{1}{2}\sum_{k,l}\frac{\partial M_{ik}}{\partial z_l} + \frac{\partial M_{il}}{\partial z_k} - \frac{\partial M_{kl}}{\partial z_i}, i = 1\ldots n\right]^T$ collects the nonlinear inertial terms i.e., the gyroscopic accelerations.

If we allow one to introduce non linear interactions between bodies of the system and external applied forces which do not derived from a potential, we will use the following more general form for the equation of motion:

$$M(z)\ddot{z} + F(t, z, \dot{z}) = 0 \tag{103}$$

where $F : I\!R^n \times I\!R^n \times I\!R \to I\!R^n$ collects the internal non linear interactions between bodies which are not necessarily derived from a potential and the external applied loads.

Summary of the equations of motion. In the sequel, the equations of motion of space-discretized continuum media and rigid bodies will be treated in the same setting. In order to summarize the equations (91), (100) and (103), we introduce the finite of variables q which can represent the discretized displacement U_h or any generalized coordinates of the rigid motion z. Hence, the equations of motion will be written as

$$M(q)\ddot{q} + F(t, q, \dot{q}) = r \tag{104}$$

where q collects the variables U_h and z.

4.2 Global to local mappings

In order to relate the global or generalized variables $q, \dot{q}$ and r to the local variables at interface $[u], \dot{U}$ and R, several global to local mappings are introduced. We assume first that the local ECZM is written on a finite number ν of geometrical points labeled by α. The assumption implies that a space discretization of the cohesive zone has been performed. If the bodies in contact are locally convex, the common point at interface can be uniquely determined and the space-discretization is straightforward. In other case, some choices have to be made to locate the points on the interface. Even in the case of rigid bodies, the procedure is not trivial and can influence the quality of numerical results.

We denote by $[u] \in \mathbb{R}^{\nu \times d}$ and $[\dot{u}] \in \mathbb{R}^{\nu \times d}$ the vectors collecting respectively the displacement and the velocity at each interface point,

$$[u] = \left[\; [\, u_N^\alpha,\, u_T^\alpha \,]_{\alpha \in \{1 \dots \nu\}} \; \right]^T, \qquad [\dot{u}] = \left[\; [\, \dot{u}_N^\alpha,\, \dot{u}_T^\alpha \,]_{\alpha \in \{1 \dots \nu\}} \; \right], \tag{105}$$

and by $\mathsf{R} \in \mathbb{R}^{\nu \times d}$ the vectors collecting the reaction R^α at each interface point,

$$\mathsf{R} = \left[\; [\, \mathsf{R}_N^\alpha,\, \mathsf{R}_T^\alpha \,]_{\alpha \in \{1 \dots \nu\}} \; \right]^T. \tag{106}$$

The local to global mappings can be written as follows

$$[u] = G(q), \tag{107}$$

$$[\dot{u}] = H(q)\dot{q}, \qquad [\dot{u}]^\alpha = H^\alpha(q)\dot{q}, \tag{108}$$

$$r = H^T(q)\mathsf{R} = \sum_\alpha H^{\alpha,T}(q)\mathsf{R}^\alpha, \tag{109}$$

where H appears as the Jacobian of the mapping G, i.e., $H = \nabla_q^T G(q)$. It is noteworthy that the relations in terms of velocities (108) and reactions (109) appears to be linear for a fixed q.

4.3 Measure differential formulation

Motivations With the presence of the unilateral constraints and dry friction or with any nonsmooth interface law, the evolution of the systems is usually no longer smooth [Brogliato,

1999]. Indeed, some nonsmoothnesses such as jumps have to be expected in the velocity and the acceleration. To take into account this particular feature of the Dynamics, some care has to be taken regarding the time derivative of kinematics variables and the definition of forces. We will see in the sequel that a rigorous mathematical framework is provided by Measure Theory.

The material of this section is inspired by the pioneering work of Jean Jacques Moreau [Moreau, 1988, 1999] on Nonsmooth Mechanics for finite-dimensional systems with unilateral constraints and Coulomb's friction. A partial presentation of the following formulation of the ECZM in a nonsmooth dynamics framework can be found in [Monerie and Acary, 2001].

The equations of motion in terms of Measure Differential Equations The velocity $v = \dot{q}$ may encounter jumps and must be considered as a function of bounded variations (B.V.) in time. Within this assumption, the equation of motion is rewritten in terms of Right continuous B.V. (R.C.B.V.) function, denoted as $v^+ = \dot{q}^+$ [1].

The generalized coordinates, assumed to be absolutely continuous, are deduced from the velocity by the standard integration of a function of bounded variations:

$$q(t) = q(t_0) + \int_{t_0}^{t} v^+(t)\, dt \tag{110}$$

where dt is the Lebesgue measure. If the velocity is a function of bounded variations, the acceleration is no longer defined everywhere as the derivative in the classical sense of the velocity. The notion of differential measure, or a special Stieltjes measure provides us with the right substitute to this notion as a derivative of the velocity in the sense of the distributions. A differential measure dv is then associated with the B.V. velocity, v as

$$dv(]a,b]) = \int_{]a,b]} dv = v^+(b) - v^+(a) \tag{111}$$

In the same way, the generalized force, r due to the unilateral constraints is also to be considered as a real-measure, denoted dp.

The equation of motion (104) is formulated in terms of a measure differential equation:

$$\begin{cases} M(q)dv + F_{int}(t,q,v^+)dt = F_{ext}(t)dt + dp \\ v^+ = \dot{q}^+ \end{cases} \tag{112}$$

If the motion is smooth with respect to time, we retrieve that $\dfrac{dv}{dt} = \dot{v} = \ddot{q}$ and $dp = rdt$. Otherwise, some jumps are expected and therefore atomic measures will be found in dv and dp.

[1] Functions of bounded variations always possess right and left limits.

Global to local mappings for measures The global to local mapping are written straightforwardly in terms of measures and right limits of B.V. function as,

$$\left\{ \begin{array}{l} [\dot{u}]^+(t) = H(q)v^+(t) \quad [\dot{u}]^{\alpha,+}(t) = H^\alpha(q)v^+(t) \\ dp = H^T(q)d\mathsf{P} = \sum_\alpha H^{\alpha,T}(q)d\mathsf{P}^\alpha \end{array} \right. \tag{113}$$

Non Smooth cohesive zone model as measures inclusion We omit in this section the index α for the sake of readability. Let us consider first the unilateral contact law,

$$-\mathsf{R}_N \in \partial I_{\mathbb{R}^+}(u_N). \tag{114}$$

This inclusion (114) is "replaced" by the following inclusion

$$-d\mathsf{P}_N \in N_{T_{\mathbb{R}^+}(u_N)}(\dot{u}_N^+(t)) \tag{115}$$

where N_C defines the normal cone to a closed convex set C, and T_C the tangent cone [Hiriart-Urruty and Lemaréchal, 1993]. This formulation is one of the keystone of the method referred as the *Moreau's sweeping process* which is a mathematical setting which combines a dynamics described in terms of measure as in (112) together with a description of the unilateral constraint including an impact law (115). The inclusion (115) will be called the inclusion in terms of velocity. Two features of this inclusion have to be mentioned: a) *the inclusion concerns measures,* b) *the inclusion in terms of velocity* $\dot{u}_N^+$ rather than of the coordinates u_N. Therefore, it is necessary to define what is the inclusion of a measure into a cone. For a mathematical definition of what is a inclusion of a measure into a cone K, we consider a nonnegative (Radon) measure $d\nu$ and we assume that the measure dr possesses a density, $r'(t) = \frac{dr}{d\nu} : [0,T] \to \mathbb{R}^\nu$ with respect to $d\nu$. The inclusion $dr \in K$ has to be understood as

$$r'(t) \in K, \quad d\nu \text{ almost everywhere.} \tag{116}$$

For more details, we refer to [Acary et al., 2006, Kunze and Monteiro Marquès, 2000, Monteiro Marques, 1993, Stewart, 2001].

Clearly, the equivalence between the inclusion in terms of velocity and the one in terms of coordinates is not ensured in the general case. A viability lemma due to Moreau [1999] ensures that the inclusion in terms of velocity (115) together with admissible initial conditions on the position implies that the constraints on the coordinates are always satisfied. In fact, we always have $N_{T_{\mathbb{R}^+}(u_N)}(\dot{u}_N^+) \subset N_{\mathbb{R}^+}(u_N)$. The reverse is clearly not true. A key assumption has to be added which is related to the notion of impact laws. Indeed, if the constraint is active, i.e. $d\mathsf{P}_N > 0$, then the post impact velocity $\dot{u_N}^+$ is equal to zero. For instance if an impact occurs, the post impact velocity vanishes. The model is a inelastic (plastic) impact rule. If the data are sufficiently smooth, we can hope that the equivalence is true if an inelastic impact rule is assumed. As it is done in [Mabrouk, 1998, Moreau, 1988], the impact rule can be enhanced with a normal coefficient of restitution e as follows

$$-d\mathsf{P}_N \in N_{T_{\mathbb{R}^+}(u_N)}(\dot{u}_N^+ + e\dot{u}_N^-). \tag{117}$$

The dry friction case is treated as well in terms of measure, i.e.,

$$-d\mathsf{P}_T \in \partial(\mu|d\mathsf{P}_N| \parallel \dot{u}_T^+ \parallel). \tag{118}$$

Finally, for the Enhanced Cohesive Zone Model in its intrinsic form (1)- (3), the measure differential inclusion is derived as

$$-d\mathsf{P}_N + d\mathsf{P}_N^{coh} \in N_{T_{\mathbb{R}^+}(u_N)}(\dot{u}_N^+ + e\dot{u}_N^-) \tag{119}$$

$$-d\mathsf{P}_T + d\mathsf{P}_T^{coh} \in \partial(\mu\,\kappa(\beta)|d\mathsf{P}_N + d\mathsf{P}_N^{coh}| \parallel \dot{u}_T^+ \parallel) \tag{120}$$

$$d\mathsf{P}^{coh} = \mathsf{R}^{coh}dt, \quad \mathsf{R}^{coh} = K(\beta)\cdot[u] \quad g(\dot{\beta},\, \beta,\, u_N,\, u_T) = 0, \tag{121}$$

where the convention $dr \in K \Leftrightarrow r' \in K$ is extended to $dr \in K(dr) \Leftrightarrow r' \in K(r')$.

Comments and interpretation If the evolution is smooth, the measure $d\mathsf{P}$ can be identified to $\mathsf{R}(t)dt$. Due to the definition of the inclusion into a cone, we retrieve the original ECZM except for the formulation of the unilateral constraint which is now in velocity. Fortunately, in smooth case, the inclusion in terms if u_N is equivalent to the inclusion in $\dot{u}_N^+(t)$. Smooth evolutions can be expected when there are no external impulses due to external impact and there are no negative relative pre-velocity. In this case, the smooth model is valid and equivalent to the nonsmooth one.

If the evolution is no longer smooth due to external impact, or the presence of unilateral contact and friction zone with negative relative velocity, a decomposition can be artificially introduced to understand what is the behavior of the model in terms of measures. Let us assume that the impulse measure $d\mathsf{P}$ can be decomposed as

$$d\mathsf{P} = \mathsf{R}dt + \mathsf{P}\delta_{t_i} \tag{122}$$

where δ_{t_i} is the Dirac distribution at time t_i and P is the amplitude of the impulse [2]. The model can be decomposed as

$$\left.\begin{array}{l} -\mathsf{R}_N + \mathsf{R}_N^{coh} \in N_{T_{\mathbb{R}^+}(u_N)}(\dot{u}_N^+ + e\dot{u}_N^-) \\ -\mathsf{R}_T + \mathsf{R}_T^{coh} \in \partial(\mu\,\kappa(\beta)|\mathsf{R}_N + \mathsf{R}_N^{coh}| \parallel \dot{u}_T^+ \parallel) \\ \mathsf{R}^{coh} = K(\beta)\cdot[u] \quad g(\dot{\beta},\, \beta,\, u_N,\, u_T) = 0 \end{array}\right\} dt\text{- almost everywhere} \tag{123}$$

and

$$\left.\begin{array}{l} -\mathsf{P}_N \in N_{T_{\mathbb{R}^+}(u_N)}(\dot{u}_N^+ + e\dot{u}_N^-) \\ -\mathsf{P}_T \in \partial(\mu\,\kappa(\beta)|\mathsf{P}_N| \parallel \dot{u}_T^+ \parallel) \\ \mathsf{P}^{coh} = 0 \end{array}\right\} \quad \text{at} \quad t = t_i \tag{124}$$

To sum up, the forces due to the cohesive interaction in the media are assumed to have only a density with the respect to the Lebesgue Measure and therefore do not enter into the model when a jump occurs. This is clearly a modeling choice which can be discussed. We will see in the next section what the consequences of this model in terms of measures on the time-discretization are.

[2] such a decomposition assumes especially that the diffuse singular measure vanishes.

5 Contact Dynamics: implicit Moreau's time stepping scheme

5.1 Time discretization of the nonsmooth dynamics

In this section, a time discretization method of the Lagrange dynamical equation (112) consistent with the nonsmooth character of the solution, is presented. This integration is inspired by the work of Moreau [1988, 1999] and Jean [1999] with some adaptations and refinements for the non linear bulk behavior and the ECZM model.

Measure differential equations Integrating both sides of this equation over a time step $]t_k, t_{k+1}]$ of length h,

$$\begin{cases} \displaystyle\int_{]t_k,t_{k+1}]} M dv + \int_{t_k}^{t_{k+1}} F(t,q,v^+)dt = \int_{]t_k,t_{k+1}]} dp, \\ q(t_{k+1}) = q(t_k) + \displaystyle\int_{t_k}^{t_{k+1}} v^+ \, dt \, . \end{cases} \tag{125}$$

where M is assumed to be constant for simplicity's sake. By definition of the differential measure dv, we have $\displaystyle\int_{]t_k,t_{k+1}]} M\, dv = M \int_{]t_k,t_{k+1}]} dv = M\,(v^+(t_{k+1}) - v^+(t_k))$. Note that the right velocities are involved in this formulation.

The impulse $\displaystyle\int_{]t_k,t_{k+1}]} dp$ of the reaction on the time interval $]t_k, t_{k+1}]$ emerges as a natural unknown. The equation of the non smooth motion can be written under an integral form as:

$$\begin{cases} M\,(v(t_{k+1}) - v(t_k)) = \displaystyle\int_{t_k}^{t_{k+1}} F(t,q,v^+)\,dt = \int_{]t_k,t_{k+1}]} dp, \\ q(t_{k+1}) = q(t_k) + \displaystyle\int_{t_k}^{t_{k+1}} v^+ \, dt \end{cases} \tag{126}$$

Since discontinuities of the derivative v are to be expected if some shocks are occurring, i.e. dp may have some Dirac atoms within the interval $]t_k, t_{k+1}]$, higher order approximations integration schemes for dp are irrelevent. It may be shown on some simple examples that, on the contrary, such high order schemes may generate spurious numerical oscillations.

The following notation is used: $q_k \approx q(t_k)$ and $q_{k+1} \approx q(t_{k+1})$, $v_k \approx v^+(t_k)$ and $v_{k+1} \approx v^+(t_{k+1})$, and

$$p_{k+1} \approx \int_{]t_k,t_{k+1}]} dp.$$

The *a priori* smooth term are evaluated with a θ-method, chosen in this context for its energy conservation ability,

$$\int_{t_k}^{t_{k+1}} F(t,q,v)\,dt \quad \approx \quad h\tilde{F}(t_k, q_k, v_k, t_{k+1}, q_{k+1}, v_{k+1}, t_{k+\theta}, q_{k+\theta}, v_{k+\theta}) \tag{127}$$

where the mid-values $t_{k+\theta}, q_{k+\theta}, v_{k+\theta}$ are defined by

$$\begin{array}{l} t_{k+\theta} = \theta t_{k+1} + (1-\theta) t_k \\ q_{k+\theta} = \theta q_{k+1} + (1-\theta) q_k \\ v_{k+\theta} = \theta v_{k+1} + (1-\theta) v_k \end{array} \quad , \quad \theta \in [0,1] \tag{128}$$

The choice of the approximated function $\tilde{F}$ strongly depends on the nature of the internal forces that are modeled. For the linear elastic behavior of homogeneous continuum media, this approximation can be made by :

$$\tilde{F}(t_k, q_k, v_k, t_{k+1}, q_{k+1}, v_{k+1}, t_{k+\theta}, q_{k+\theta}, v_{k+\theta}) = \frac{1}{2} K : [E(q_k) + E(q_{k+1})] : F(q_{k+1/2}) \tag{129}$$

which leads to a energy conserving algorithm as in [Simo and Tarnow, 1992]. For nonlinear elastic other smooth non linear behaviors, we refer to the work of Gonzalez [2000], Laursen and Meng [2001] for the choice of the discretization and the value of θ.

The displacement, assumed to be absolutely continuous is approximated by:

$$q_{k+1} = q_k + h\, v_{k+\theta} \, .$$

The following time discretized equation of motion is obtained:

$$\begin{cases} M(v_{k+1} - v_k) + h\tilde{F}(t_k, q_k, v_k, t_{k+1}, q_{k+1}, v_{k+1}, t_{k+\theta}, q_{k+\theta}, v_{k+\theta}) = p_{k+1} \\ q_{k+1} = q_k + h v_{k+\theta} \end{cases} \tag{130}$$

which is assumed to be linearized and iteratively solved at each time by for instance a Newton procedure or one of its variants. The linearized system will be denoted as

$$\begin{cases} (M + h\theta C_t + \theta^2 h^2 K_t)(v_{k+1} - v_k) + \phi(t_k, q_k, v_k) = p_{k+1} \\ q_{k+1} = q_k + h v_{k+\theta} \end{cases} \tag{131}$$

where the matrices C_t and K_t stand for the tangent viscous and stiffness matrices.

For $\theta = 0$, the scheme is explicit in the evaluation of the internal forces. When loading or fracture are highly dynamical, it may be interesting to use such a scheme with small time-steps avoiding the evaluation of the tangent operators. We retrieve in the case a scheme which is very similar to the scheme of Carpenter et al. [1992]. For $\theta \in]0,1]$, we obtain a semi-implicit scheme with good stability property for $\theta \geqslant 1/2$. With $\theta = 1/2$, a second order in accuracy can be retrieved in smooth evolution. It is noteworthy that whatever how the parameter θ is chosen, the scheme is fully implicit for the evaluation of the reaction impulses dp.

Global to local mappings The global to local mappings are discretized in a fully implicit way for the terms involving velocities and impulses :

$$[\dot{u}]_{k+1} = H(\tilde{q}_{k+1}) \dot{q}_{k+1}, \tag{132}$$

$$p_{k+1} = H^T(\tilde{q}_{k+1}) \mathsf{P}_{k+1} = \sum_\alpha H^{\alpha,T}(\tilde{q}_{k+1}) \mathsf{P}^\alpha_{k+1}. \tag{133}$$

For the displacement, two parameters γ_1, γ_2 are introduced to forecast the configuration at contact as

$$\tilde{q}_{k+1} = q_k + h(\gamma_1 v_k + \gamma_2 v_{k+1}) \tag{134}$$

For most applications in which the normal to the interface do not change too quickly or if the curvatures of the interface are small, the evaluation of the contact configuration may be explicit, that is $\gamma_2 = 0$ and γ_1 is chosen in $[0, 1]$.

5.2 Time discretization of the ECZM

Finally, the ECZM model in discretized in a implicit way,

$$\begin{aligned}
&-\mathsf{P}_{N,k+1} + \mathsf{P}^{coh}{}_{N,k+1} \in N_{T_{\mathbb{R}^+}(\tilde{u_{N}}_{k+1})}([\dot{u}]_{N,k+1} + e[\dot{u}]_{N,k}) \\
&-\mathsf{P}_{T,k+1} + \mathsf{P}^{coh}{}_{T,k+1} \in \partial(\mu\,\kappa(\beta_{k+1})|\mathsf{P}_{N,k+1} + \mathsf{P}^{coh}{}_{N,k+1}| \parallel [\dot{u}]_{T,k+1} \parallel) \\
&\mathsf{P}^{coh}{}_{k+1} = h\mathsf{R}^{coh}_{k+1}, \quad \mathsf{R}^{coh}_{k+1} = K(\beta_{k+1}) \cdot [u]_{k+1} \quad \hat{g}(\dot{\beta}_{k+1},\, \beta_{k+1}, \beta_k,\, [u]_{N,k+1}, [u]_{T,k+1}) = 0
\end{aligned} \tag{135}$$

where the function $\hat{g}$ is the numerical counterpart of the function $\tilde{g}$ evaluated at the discrete approximations of the variables, $\dot{\beta}, \beta, u_N, u_T$. The displacement jump $\tilde{u_{N}}_{k+1}$ is evaluated in a consistent manner with respect to (134),

$$\tilde{u_{N}}_{k+1} = u_{Nk} + h(\gamma_1[\dot{u}]_{N,k} + \gamma_2[\dot{u}]_{N,k+1}). \tag{136}$$

An obvious choice for γ_1 and γ_2 is to be coherent with the forecast of the generalized displacement as in (134). In the same way, the approximation of the displacement jump $[u]_{k+1}$ can be derived directly from the global to local mappings and the approximation (131). Nonetheless, some other choices can also be suitable for ensuring gap consistency, for instance, or the conservation of energy at impact in the elastic case. In this case, the displacement jump $[u]_{k+1}$ is approximated from the local relative velocities $[\dot{u}]_{N,k}$ and $[\dot{u}]_{N,k+1}$ with a different numerical integration rule. For a comprehensive discussion of this point we refer to [Jean, 1999].

A substantial discrepancy has to be noted between the time integration of the impulses P and the smooth reaction R. For the impulses, the total amplitude of the impulses is conserved as primary variable. For the smooth reaction forces, the time discretization is given by a implicit rule.

Finally, the systems of inclusions (135) is rewritten in terms of conditional complementarity conditions for computational purposes as

$$\text{if } \tilde{u_N}_{k+1} > 0, \text{ then} \qquad \mathsf{P}_{N,k+1} - \mathsf{P}^{coh}{}_{N,k+1} = 0$$

$$\text{if } \tilde{u_N}_{k+1} \leqslant 0, \text{ then} \qquad 0 \leqslant \mathsf{P}_{N,k+1} - \mathsf{P}^{coh}{}_{N,k+1} \perp [\dot{u}]_{N,k+1} + e[\dot{u}]_{N,k} \geqslant 0$$

$$-\mathsf{P}_{T,k+1} + \mathsf{P}^{coh}{}_{T,k+1} \in \partial(\mu\,\kappa(\beta_{k+1})|\mathsf{P}_{N,k+1} + \mathsf{P}^{coh}{}_{N,k+1}| \parallel [\dot{u}]_{T,k+1} \parallel)$$

$$\mathsf{P}^{coh}{}_{k+1} = h\mathsf{R}^{coh}_{k+1}, \quad \mathsf{R}^{coh}_{k+1} = K(\beta_{k+1}) \cdot [u]_{k+1} \quad \hat{g}(\dot{\beta}_{k+1},\, \beta_{k+1}, \beta_k,\, [u]_{N,k+1}, [u]_{T,k+1}) = 0 \tag{137}$$

5.3 Numerical scheme and algorithm

Local formulation of the problem. The resolution of the discretized and linearized problem is based on a condensation on local variables of the dynamical equation (131) using the equations (132)–(133). The reduced equation of the Dynamics can be read as

$$[\dot{u}]_{k+1} = [\dot{u}]_{free} + WP_{k+1} \tag{138}$$

where the matrix, called the Delassus operator,

$$W = H(\tilde{q}_{k+1})(M + h\theta C_t + \theta^2 h^2 K_t)^{-1})H^T(\tilde{q}_{k+1}),$$

models the local behavior of the bodies at the interface, and the vector

$$v_{free} = H(\tilde{q}_{k+1})(v_k - (M + h\theta C_t + \theta^2 h^2 K_t)^{-1}\phi(t_k, q_k, v_k))$$

is the relative free velocity, that is the velocity without the contribution of the ECZM.

At each Newton step the following system has to be solved :

$$[\dot{u}]_{k+1} = [\dot{u}]_{free} + WP_{k+1}$$

$$-\mathsf{P}_{N,k+1} + \mathsf{P}^{coh}{}_{N,k+1} \in N_{T_{\mathbb{R}^+}(\tilde{u_N}_{k+1})}([\dot{u}]_{N,k+1} + e[\dot{u}]_{N,k})$$

$$-\mathsf{P}_{T,k+1} + \mathsf{P}^{coh}{}_{T,k+1} \in \partial(\mu\,\kappa(\beta_{k+1})|\mathsf{P}_{N,k+1} + \mathsf{P}^{coh}{}_{N,k+1}| \parallel [\dot{u}]_{T,k+1} \parallel)$$

$$\mathsf{P}^{coh}{}_{k+1} = h\mathsf{R}^{coh}_{k+1}, \quad \mathsf{R}^{coh}_{k+1} = K(\beta_{k+1}) \cdot [u]_{k+1} \quad \hat{g}(\dot{\beta}_{k+1},\, \beta_{k+1}, \beta_k,\, [u]_{N,k+1}, [u]_{T,k+1}) = 0 \tag{139}$$

Local resolution. The procedure which is used to solve the previous problem is based on an algorithm already extensively used for the tridimensional contact problem. Indeed, we define the following variable:

$$-\tilde{\mathsf{P}}_{N,k+1} = -\mathsf{P}_{N,k+1} + \mathsf{P}^{coh}{}_{N,k+1}, -\tilde{\mathsf{P}}_{T,k+1} = -\mathsf{P}_{T,k+1} + \mathsf{P}^{coh}{}_{T,k+1} \tag{140}$$

the following systems of equations is solved assuming known provisional values for ${\mathsf{P}^{coh}}_{k+1}, \beta_{k+1}$ and $[u]_{k+1}$,

$$\begin{cases} [\dot{u}]_{k+1} = [\dot{u}]_{free} + W P_{k+1} \\ -\tilde{\mathsf{P}}_{N,k+1} \in N_{T_{\mathbb{R}^+}(\tilde{u_N}_{k+1})}([\dot{u}]_{N,k+1} + e[\dot{u}]_{N,k}) \\ -\tilde{\mathsf{P}}_{T,k+1} \in \partial(\mu\, \kappa(\beta_{k+1})|\tilde{\mathsf{P}}_{N,k+1}| \parallel [\dot{u}]_{T,k+1} \parallel) \end{cases} \tag{141}$$

This last system is a standard discretized system for tridimensional unilateral contact and friction. The numerical algorithm is derived from standard splitting algorithm for Linear and non linear Complementarity problem which are well suited for large systems of equations. Each subproblem is solved by a nonsmooth Newton solver. More details can be found in [Alart and Curnier, 1991, Jean, 1999, Jourdan et al., 1998].

Update of the cohesive variables ${\mathsf{P}^{coh}}_{k+1}, \beta_{k+1}$ and local displacement $[u]_{k+1}$. Three methods are used for the update of the cohesive variables. The first one is based on a fixed point procedure. The values of ${\mathsf{P}^{coh}}_{k+1}, \beta_{k+1}, [u]_{k+1}$ are updated after the resolution of the pure contact friction problem (141) with an iterative splitting algorithm. The second one considers β as internal state variable and is updated in the Newton loop. Finally, a third procedure uses directly the iterative splitting algorithms and leaves the non linearity due to the cohesive laws to the contact-friction algorithm.

6 Conclusion

In this paper, the concept of enhanced cohesive zone dedicated to the nonsmooth fracture dynamics is presented. This concept allows us to extend any extrinsic or intrinsic cohesive zone model with the frictional and unilateral conditions which are well suited to the dynamic fracture of homogeneous, heterogeneous and graded materials. Some theoretical and practical uses of this concept together with the cohesive-volumetric finite element approach are investigated. A particular attention is paid to two main limitations of the cohesive zone models often emphasized in the literature: (i) instabilities or solution jumps related to the softening behavior of the extrinsic or intrinsic cohesive zone models, and (ii) the mesh sensitivity of the solution. A wide analysis of the first point in the quasi-static case shows that the cohesive zone models are equivalent one to each other for stable rectilinear crack propagation, but not for the crack initiation and the crack branching. In particular, a quantitative explanation of the fact that the extrinsic models are more stable the intrinsic models is given. The interest of an accurate dynamical relaxation, namely the nonsmooth contact dynamics method, is illustrated on a local graph (condensed problem). For the second point, the notion of 'mesh sensitivity' is clarified: although the spatial convergence of the crack path is not reached for 'crossed-triangle quadrilateral' meshes [Tijssens et al., 2000], it is reached for meshes having the 'isoparametric properties' [Papoulia et al., 2006]; moreover,

the independence of the overall elastic and fracture properties to the mesh size is obtained when a new micromechanical-based criterion on a cohesive internal length is satisfied.

In a second part of this paper, a comprehensive formulation of a nonsmooth dynamical framework is provided. This framework based on measure differential inclusions allows one to take into account the nonsmooth evolutions. This mathematical background leads to a sound numerical method for solving the nonsmooth fracture dynamics in a consistent way. In a forthcoming article, more illustrations will be given on the ability of this method to simulate real-like applications.

References

F.F. Abraham. How fast can cracks move? a research adventure in materials failure using millions of atoms and big computers. *Advances in Physics*, 52(8), 2003.

F.F. Abraham, D. Brodbeck, W.E. Rudge, J.Q. Broughton, D. Schneider, B. Land, D. Lifka, J. Gerner, M. Rosenkrantz, J. Skovira, and H. Gao. Ab initio dynamics of rapid fracture. *Modelling and Simulation in Materials Science and Engineering*, 6:639–670, 1998.

F.F. Abraham, N. Bernstein, J.Q. Broughton, and D. Hess. Dynamic fracture of silicon: concurrent simulation of quantum electrons, classical atoms, and the continuum solid. *MRS Bulletin*, 25:27–32, 2000.

V. Acary, B. Brogliato, and D. Goeleven. Higher order Moreau's sweeping process: Mathematical formulation and numerical simulation. *Mathematical Programming A*, 2006. To appear, INRIA Research report available at http://www.inria.fr/rrrt/rr-5236.html.

P. Alart and A. Curnier. A mixed formulation for frictional contact problems prone to Newton like solution method. *Computer Methods in Applied Mechanics and Engineering*, 92(3):353–375, 1991.

O. Allix, P. Ladevèze, and A. Corigliano. Damage analysis of interlaminar fracture specimens. *Composite Structures*, 31(1):61–74, 1995.

C. Atkinson and J.D. Eshelby. The flow energy into the tip of a moving crack. *Int. J. Fract.*, 4:3–8, 1968.

G.I. Barenblatt. The mathematical theory of equilibrium cracks in brittle fracture. *Adv. Appl. Mech.*, 7:55–129, 1962.

B. Brogliato. *Nonsmooth Mechanics: Models, Dynamics and Control.* Communications and Control Engineering. Springer-Verlag, second edition, 1999.

G.T. Camacho and M. Ortiz. computational modelling of impact damage in brittle materials. *International Journal of Solids and Structures*, 33:2899–2938, 1996.

N.J. Carpenter, R.L. Taylor, and M.G. Katona. Lagrange constraints for transient finite element surface contact. *International Journal for Numerical Methods in Engineering*, 32: 103–108, 1992.

J.-L. Chaboche, R. Girard, and P. Levasseur. On the interface debonding models. *Int. J. Damage Mechanics*, 6:220–257, 1997.

J.-L. Chaboche, F. Feyel, and Y. Monerie. Interface debonding model: a viscous regularization with a limited rate dependency. *Int. J. Solids Structures*, 38:3127–3160, 2001.

N. Chandra, H. Li, C. Shet, and H. Ghonem. Some issues in the application of cohesive zone models for metal-ceramic interfaces. *Int. J. Solids Structures*, 39:2827–2855, 2002.

M. Cocu, E. Pratt, and M. Raous. Formulation and approximation of quasistatic frictional contact. *Int. J. Eng. Sci.*, 34(7):783–798, 1996.

F. Costanzo and J.R. Walton. A study of dynamic crack growth in elastic materials using a cohesive zone model. *Int. J. Engng Sci.*, 35(12-13):1085–1114, 1997.

D.R. Curran, L. Seaman, and D.A. Shockey. Dynamic failure of solids. *Phys. Rep.*, 147: 253–388, 1987.

J.W. Dally. Dynamic photoelastic studies of fracture. *Exp. Mech.*, 19:349–361, 1979.

R. de Borst, J.J.C. Remmers, and A. Needleman. Mesh-independent discrete numerical representations of cohesive-zone models. *Enginnering Fracture Mechanics*, 73:160–177, 2006.

D.S. Dugdale. Yielding of steel sheets containing slits. *J. Mech. Phys. Solids*, 8:100–104, 1960.

H.D. Espinosa and N.S. Brar. Dynamic failure mechanisms of ceramic bars: experiments and numerical simulations. *Journal of the Mechanics and Physics of Solids*, 43:1615–1638, 1995.

H.D. Espinosa and P.D. Zavattieri. A grain level model for the study of failure initiation and evolution in polycrystalline brittle materials. Part I:Theory and numerical implementation. *Mechanics of Materials*, 35:333–364, 2003.

M.L. Falk, A. Needleman, and J.R. Rice. A critical evaluation of dynamic fracture simulations using cohesive surfaces. *Journal de Physique IV*, 11:43–52, 2001.

J. Fineberg and M. Mader. Instability in dynamic fracture. *Physics Reports*, 313:1–108, 1999.

M. Frémond. Adhésion et contact unilatéral. In *Contact mechanics and wear of rail/wheel systems*, pages 63–77, Vancouver British Columbia, July 6-9 1982. University of Waterloo Press.

M. Frémond. Contact unilatéral avec adhérence, une théorie du premier gradient. In G. Del Piero and F. Maceri, editors, *Unilateral Problems in Structural Analysis*, volume 304 of *CISM - Courses and Lectures*, pages 117–137, Prescudin, june 17-20 1985. Preceedings of the $2^n d$ meeting on Unilateral Problems in Structural Analysis.

M. Frémond. Adhérence des solides. *Journal de Mécanique Théorique et Appliquée*, 6(3): 383–407, 1987.

M. Frémond. Contact with adhesion. In J.-J. Moreau and P.D. Panagiotopoulos, editors, *Nonsmooth mechanics and applications*, volume 302 of *CISM - Courses and Lectures*, pages 177–221. Springer, 1988.

L.B. Freund. *Dynamic fracture mechanics*. Cambridge University Press, 1990.

H. Gao and P. Klein. Numerical simulation of crack growth in an isotropic solid with randomized internal cohesive bonds. *J. Mech. Phys. Solids*, 46:187–218, 1998.

J.-M. Gatt, Y. Monerie, D. Laux, and D. Baron. Elastic behavior of porous ceramics: application to nuclear fuel materials. *Journal of Nuclear Materials*, 336:145–155, 2005.

P. Germain, Q.S. Nguyen, and P. Suquet. Continuum thermodynamics. *ASME Journal of Applied Mechanics*, 50, 50th Anniversary Issue:1010–1020, 1983.

P.H. Geubelle and J.S. Baylor. Impact-induced delamination of composites: A 2d simulation. *Composites Part B: Engineering*, 29:589–602, 1998.

O. Gonzalez. Exact energy and momentum conserving algorithms for general models in nonlinear elasticity. *Computer Methods in Applied Mechanics and Engineering*, 190:1762–1783, 2000.

D.E. Grady and M.E. Kipp. Dynamic fracture and fragmentation. In J.R. Asay and M. Shahinpoor, editors, *High-Pressure Shock Compression of Solids*, pages 265–322. Springer-Verlag, New York, 1993.

A.A. Griffith. The phenomenon of rupture and flow in solids. *Philosophical Transaction of the Royal Society (London)*, A221:163–198, 1920.

Z. Hashin and S. Shtrikman. A variational approach to the theory of the elastic behaviour of multiphase materials. *J. Mech. Phys. Solids*, 11:127–140, 1963.

J.B. Hiriart-Urruty and C. Lemaréchal. *Convex Analysis and Minimization Algorithms*, volume I et II. Springer Verlag, Berlin, 1993.

Y. Ida. Cohesive force across the tip of a longitudinal shear crack and Griffith's specific surface energy. *Journal of Geophysical Research*, 77:3796–3805, 1972.

M. Jean. The non smooth contact dynamics method. *Computer Methods in Applied Mechanics and Engineering*, 177:235–257, 1999. Special issue on computational modeling of contact and friction, J.A.C. Martins and A. Klarbring, editors.

Z.-H. Jin, G. H. Paulino, and R. H. Dodds Jr. Finite element investigation of quasi-static crack growth in functionally graded materials using a novel cohesive zone fracture model. *Journal of Applied Mechanics*, 69:370–379, 2002.

F. Jourdan, P. Alart, and M. Jean. A Gauss–Seidel-like algorithm to solve frictional contact problems. *Computer Methods in Applied Mechanics and Engineering*, 155(1):31–47, 1998.

N. Kikuchi and J.T. Oden. *Contact problems in elasticity : a study of variational inequalities and finite element methods.* SIAM, Philadelphia, 1988.

P. Klein and H. Gao. Crack nucleation and growth as strain localization in a virtual-bond continuum. *Eng. Fract. Mech.*, 61:21–48, 1998.

D.K. Kubair and P. Geubelle. Comparative analysis of extrinsic and intrinsic cohesive models of dynamic fracture. *Int. J. Solids Structures*, 40:3853–3868, 2003.

M. Kunze and M.D.P. Monteiro Marquès. An introduction to Moreau's sweeping process. In B. Brogliato, editor, *Impact in Mechanical systems: Analysis and Modelling*, volume 551 of *Lecture Notes in Physics*, pages 1–60. Springer, 2000.

T.A. Laursen and X.N. Meng. A new solution procedure for application of energy-conserving algorithms to general constitutive models in nonlinear elastodynamics. *Computer Methods in Applied Mechanics and Engineering*, 190:6309–6322, 2001.

S. Li, M.D. Thouless, A.M. Waas, J.A. Schroeder, and P.D. Zavattieri. Mixed-mode cohesive-zone models for fracture of an adhesively bonded polymer-matrix composite. *Engineering Fracture Mechanics*, 73:64–78, 2006.

M. Mabrouk. A unified variational for the dynamics of perfect unilateral constraints. *European Journal of Mechanics. A/ Solids.*, 17:819–842, 1998.

J.-C. Michel and P. Suquet. An analytical and numerical study of the overall behaviour of metal-matrix composites. *Modelling Simul. Mater. Sci.*, 2:637–658, 1994.

J.-C. Michel, P. Suquet, and F. Thébaud. Une étude théorique et numérique de la décohésion d'interface dans les composites à matrice metallique et renfort particulaire. In O. Allix, J.-P. Favre, and P. Ladeveze, editors, *Comptes Rendus des Huitièmes Journées Nationales sur les Composites*, pages 835–846. AMAC, 1992.

Y. Monerie. *Fissuration des matériaux composites : rôle de l'interface fibre/matrice.* PhD thesis, Université Aix-Marseille II, 2000.

Y. Monerie and V. Acary. Formulation dynamique d'un modèle de zone cohésive tridimensionnel couplant endommagement et frottement. *Revue Eur. Eléments Finis*, 10:489–504, 2001.

Y. Monerie, F.H. Leroy, O. Sudre, F. Feyel, and J.L. Chaboche. Comparaison de lois d'interface fibre/matrice sur la base d'un modèle uniaxial d'expérience de micro-indentation. In J. Lamon and D. Baptiste, editors, *Comptes Rendus des Onzièmes Jounées Nationales sur les Composites*, volume II, pages 565–574, Arcachon, 18-20 Novembre 1998. AMAC.

M. D. P. Monteiro Marques. *Differential Inclusions in NonSmooth Mechanical Problems : Shocks and Dry Friction.* Birkhauser, Verlag, 1993.

J.J. Moreau. Unilateral contact and dry friction in finite freedom dynamics. In J.J. Moreau and P.D. Panagiotopoulos, editors, *Nonsmooth Mechanics and Applications*, number 302 in CISM, Courses and lectures, pages 1–82. CISM 302, Spinger Verlag, Wien- New York, 1988. Formulation mathematiques tire du livre Contacts mechanics.

J.J. Moreau. Numerical aspects of the sweeping process. *Computer Methods in Applied Mechanics and Engineering*, 177:329–349, 1999. Special issue on computational modeling of contact and friction.

T Mura. *Micromechanics of defects in solids.* Martinus Nijhoff, 1982.

A. Needleman. A continuum model for void nucleation by inclusion debonding. *Journal of Applied Mechanics*, 54:525–531, 1987.

A. Needleman. An analysis of tensile decohesion along an interface. *J. Mech. Phys. Solids*, 38(3):289–324, 1990.

A. Needleman. Micromechanical modeling of interfacial decohesion. *Ultramicroscopy*, 40: 203–214, 1992.

A. Needleman and A.J. Rosakis. The effect of bond strenght and loading rate on the conditions governing the attainment of intersonic crack growth along interfaces. *J. Mech. Phys. Solids*, 47:2411–2450, 1999.

M. Ortiz and A. Pandolfi. Finite-deformation irreversible cohesive elements for three-dimensional crack-propagation analysis. *International Journal for Numerical Methods in Engineering*, 44:1267–1282, 1999.

M. Ortiz and L. Stainier. The variational formulation of viscoplastic constitutive updates. *Comp. Meth. Appl. Mech. Eng.*, 171:419–444, 1999.

A.C. Palmer and J.R. Rice. The growth of slip surfaces in the progressive failure of over-consolidated clay. *Proceedings of the Royal Society (London)*, A332:527–548, 1973.

A. Pandolfi, P.R. Guduru, M. Ortiz, and A.J. Rosakis. Three dimensional cohesive-element analysis and experiments of dynamic fracture in c300 steel. *International Journal of Solids and Structures*, 37:3733–3760, 2000.

K. Papoulia, S. Vavasis, and P. Ganguly. Spatial convergence of crack nucleation using a cohesive finite element model on a pinwheel-based mesh. *International Journal for Numerical Methods in Engineering*, 67:1–16, 2006.

F. Perales. *Fissuration des matériaux à gradient de propriétés. Application au Zircaloy hydruré.* PhD thesis, Université Montpellier II, 2005.

F. Perales, Y. Monerie, F. Dubois, and L. Stainier. Computational non-smooth fracture dynamics in nonlinear and heterogeneous materials. Application to fracture of hydrided Zircaloy. In Y. Zhou, S. Yu, and Y. Xu, editors, *Structural Mechanics In Reactor Technology*, volume 18, Beijing, China, 2005. Atomic Energy Press.

N. Point. Unilateral contact with adherence. *Mathematical Methods in the Applied Sciences*, 10:367–381, 1988.

N. Point and E. Sacco. Mathematical properties of a delamination model. *Mathematical and computer modelling*, 28(4–8):359–371, 1998.

M. Raous and Y. Monerie. Unilateral contact, friction and adhesion : 3D crack in composite material. In J.A.C Martins and Monteiro Marques M.D.P, editors, *3d Contact Mechanics International Symposium*, Collection Solid Mechanics and its Applications, pages 333–346. Kluwer, Peniche (Portugal), 17-21 june 2001.

M. Raous, L. Cangémi, and M. Cocu. Consistent model coupling adhesion, friction and unilateral contact. *Computer Meth. Appl. Mech. and Engrg.*, 177(3-4):383–399, 1999.

J.J.C. Remmers, R. de Borst, and A. Needleman. A cohesive segments method for the simulation of crack growth. *Computational Mechanics*, 31:69–77, 2003.

J. R. Rice and J.-S. Wang. Embrittlement of interfaces by solute segregation. *Materials Science and Engineering A: Structural Materials: Properties, Microstructure and Processing*, A107:23–40, 1989.

J.R. Rice. Mathematical analysis in the mechanics of fracture. In H. Liebowitz, editor, *Fracture, an Advanced Treatise*, volume 2, pages 191–311. Academic Press, New York, 1968.

J.H. Rose, J. Ferrante, and J.R. Smith. Universal binding energy curves for metals and bimetallic interfaces. *Phys. Rev. Lett.*, 47:675–678, 1981.

J.H. Rose, J.R. Smith, and J. Ferrante. Universal features of bonding in metals. *Phys. Rev.*, B28:1835–1845, 1983.

R.E. Rudd and J.Q. Broughton. Coarse-grained molecular dynamics and the atomic limit of finite elements. *Physical Review B*, 58:R5893–R5896, 1998.

L. Seaman, D.R. Curran, and W.J. Murri. A continuum model for dynamic tensile microfracture and fragmentation. *J Appl Mech*, 52:593–600, 1985.

T. Siegmund and A. Needleman. A numerical study of dynamic crack growth in elastic-viscoplastic solids. *Int. J. Solids Structures*, 34(7):769–787, 1997.

T. Siegmund, N.A. Fleck, and A. Needleman. Dynamic crack growth across an interface. *International Journal of Fracture*, 85:381–402, 1997.

J.C. Simo and N. Tarnow. The discrete energy-momentum method. conserving algorithms for nonlinear elastodynamics. *Zeitschrift für Angewandte Mathematik und Physik*, 43: 757–792, 1992.

D. Stewart. Reformulations of measure differential inclusions and their closed graph property. *Journal of Differential Equations*, 175(1):108–129, 2001.

Z. Suo, M. Ortiz, and A. Needleman. Stability of solids with interfaces. *J. Mech. Phys. Solids*, 40(3):613–640, 1992.

Z. Suo, C.F. Shih, and A.G. Varias. A theory of cleavage cracking in the presence of plastic flow. *Acta Met.*, 41:1551–1557, 1993.

G. Thiagarajan and A. Misra. Fracture simulation for anisotropic materials usign a virtual internal bond model. *International Journal of Solids and Structures*, 41:2919–2938, 2004.

M.G.A. Tijssens, L.J. Sluys, and E. van der Giessen. Numerical simulation of quasi-brittle fracture using damaging cohesive surface. *Eur. J. Mech. A/Solids*, 19:761–779, 2000.

V. Tvergaard. Effect of fibre debonding in a whisker-reinforced metal. *Materials Science and Engineerging*, A125:203–213, 1990.

V. Tvergaard. Effect of thermally induced residual stresses on the failure of a whisker-reinforced metal. *Mechanics of Materials*, 11:149–161, 1991.

V. Tvergaard and J.W. Hutchinson. The relation between crack growth resistance and fracture process parameters in elastic-plastic solids. *J. Mech. Phys. Solids*, 40:1377–1397, 1992.

V. Tvergaard and J.W. Hutchinson. Effect of strain-dependent cohesive zone model on predictions of crack growth resistance. *Int. J. Solids Struct.*, 33:3297–3308, 1996.

A.G. Varias and A.R. Massih. Hydride-induced embrittlement and fracture in metals - effect of stress and temperature distribution. *Journal of the Mechanics and Physics of Solids*, 50:1469–1510, 2002.

Z. Wang and T. Nakamura. Simulations of crack propagation in elastic-plastic graded materials. *Mechanics of Materials*, 36:601–622, 2004.

Y. Wei and J.W. Hutchinson. Models of interface separation accompanied by plastic dissipation at multiple sclaes. *Int. J. Fract.*, 95:1–17, 1999.

J.R. Willis. A comparison of the fracture criteria of Griffith and Barenblatt. *J. Mech. Phys. Solids*, 15:151–162, 1967.

J.R. Willis. Equations of motions for propagating cracks. *The Mechanics and Physics Fracture*, pages 57–67, 1975.

L.R. Xu, Y.Y. Huang, and A.J. Rosakis. Dynamic crack deflection and penetration at interfaces in homogeneous materials: experimental studies and model predictions. *J. Mech. Phys. Solids*, 51:461–486, 2003.

X.-P. Xu and A. Needleman. Numerical simulations of fast crack growth in brittle solids. *J. Mech. Phys. Solids*, 42(9):1397–1434, 1994.

X.-P. Xu, A. Needleman, and F.F. Abraham. Effect of inhomogeneities on dynamic crack growth in an elastic solid. *Modelling Simul. Mater. Sci. Eng.*, 5:489–516, 1997.

P.D. Zavattieri and H.D. Espinosa. Grain level analysis of crack initiation and propagation in brittle materials. *Acta Materialia*, 49:4291–4311, 2001.

Z.J. Zhang and G.H. Paulino. Cohesive zone modeling of dynamic failure in homogeneous and functionally graded materials. *International Journal of Plasticity*, 21:1195–1254, 2005.

Unité de recherche INRIA Rhône-Alpes
655, avenue de l'Europe - 38334 Montbonnot Saint-Ismier (France)

Unité de recherche INRIA Futurs : Parc Club Orsay Université - ZAC des Vignes
4, rue Jacques Monod - 91893 ORSAY Cedex (France)
Unité de recherche INRIA Lorraine : LORIA, Technopôle de Nancy-Brabois - Campus scientifique
615, rue du Jardin Botanique - BP 101 - 54602 Villers-lès-Nancy Cedex (France)
Unité de recherche INRIA Rennes : IRISA, Campus universitaire de Beaulieu - 35042 Rennes Cedex (France)
Unité de recherche INRIA Rocquencourt : Domaine de Voluceau - Rocquencourt - BP 105 - 78153 Le Chesnay Cedex (France)
Unité de recherche INRIA Sophia Antipolis : 2004, route des Lucioles - BP 93 - 06902 Sophia Antipolis Cedex (France)

Éditeur
INRIA - Domaine de Voluceau - Rocquencourt, BP 105 - 78153 Le Chesnay Cedex (France)
http://www.inria.fr
ISSN 0249-6399